Use Authorization

In presenting this thesis in partial fulfillment of the requirements for an advanced degree at Idaho State University, I agree that the library shall make it freely available for inspection. I further state that permission for extensive copying of my thesis for scholarly purposes may be granted by the Dean of the Graduate School, Dean of my academic division, or by the University Librarian. It is understood that any copying or publication of this thesis for financial gain shall not be allowed without my written permission.

Signature _____

Date _____

Bison Fuel Performance Code Fuel Fracture Validation

by

Casey Steinman

A thesis

submitted in partial fulfillment

of the requirements for the degree of

Master of Science in the Department of Communication Sciences and Disorders

Idaho State University

Summer 2021

To the Graduate Faculty:

The members of the committee appointed to examine the thesis of Casey Steinman find it satisfactory and recommend that it be accepted.

_____

Dr. Mary Lou Dunzik-Gougar,

Major Advisor

_____

Dr. Benjamin Spencer,

Committee Member

_____

Dr. Leslie Kerby,

Graduate Faculty Representative

Contents

List of Figures

Bison Fuel Performance Code Fuel Fracture Validation

Thesis Abstract—Idaho State University (2021)

Due to thermal expansion of nuclear fuel pellets the thermal gradient created in a light water reactor environment will cause fuel pellets to crack on their initial ramp to power. This multi-institutional project uses three experiments to reproduce the thermal gradient created in a light water reactor, a resistive heating experiment, a quenching experiment, and one using the transient testing reactor. The Bison fuel performance code has several fuel crack modeling approaches built into the code that need to be validated. Two approaches, the smeared cracking approach and extended finite element method, were used in this project to model the experiments and validate the Bison fuel performance code. The quenching experiment has run several trials for comparison to the modeled results. These experiments have been compared to models using the smeared cracking approach.

Key Words:

Bison fuel performance code

Validation

Uranium dioxide cracking

Chapter 1. Introduction

a. Motivation

The Bison fuel performance code employs several simulation techniques for modeling fuel fracturing in a light water reactor environment. Validation of these models has proven challenging largely due to a lack of meaningful, quantitative data. There is no consensus on what parameters should be measured and how to measure them. The work presented in this thesis is part of a larger project with the objectives to design and perform fuel cracking experiments and to use the experimental data to validate Bison's fuel cracking models. Cracking occurs in new LWR fuel during its initial use, before any swelling or bambooing. This cracking occurs solely due to the temperature profile across the fuel pellet, which is much higher in the center and drops sharply toward edges. Three types of experiments were designed and conducted to reproduce that temperature profile and cause cracking in UO2 pellets. These experiments were performed at the University of South Carolina, Texas A&M University and Idaho National Lab. The university-based experiments were out-of-pile, using two different approaches to create the temperature profile. The University of South Carolina pursued resistive heating of the pellet, while cold bath quenching of a heated pellet was the Texas A&M approach. An in-pile experiment was performed at the transient test reactor facility (TREAT) at Idaho National Lab. This thesis focuses on models used to inform the design of the quenching and TREAT experiments, as well as quenching experiment data analysis.

Chapter 2. Background

a. Fuel Thermal Mechanics

i. Thermal Expansion and Thermal Conductivity

During Normal operation of a nuclear reactor uranium dioxide, or UO_2, fuel pellets will crack (Chiang, & Faya 1961). This cracking directly effects the performance of the fuel pellet including heat transfer from the pellet (Van Brutzel, Dingerville, & Bartel, 2015). Two properties that play an important role in fuel pellet cracking are thermal expansion and thermal conductivity. Both of these properties are temperature dependent, but to different degrees (UCHIDA, SUNAOSHI, KATO, & KONASHI, 2011). The thermal expansion coefficient is less affected by temperature. It ranges from roughly $1*10^{-5}$ to $2.1*10^{-5}$ 1/K between 500 and 2500 K (roughly a factor of 2) as shown in figure 1.

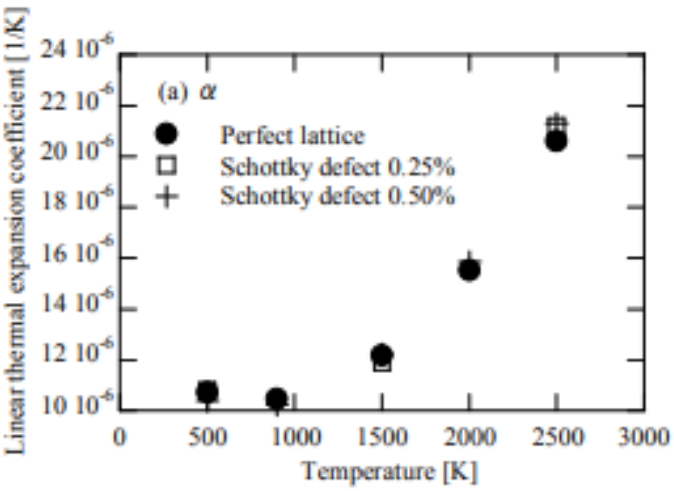

Figure 1. Thermal Expansion Coefficient of UO_2 (UCHIDA, SUNAOSHI, KATO, & KONASHI, 2011)

The heat transfer coefficient values vary by up to a factor of 5 or more across the same temperature range as can be seen in figure 2.

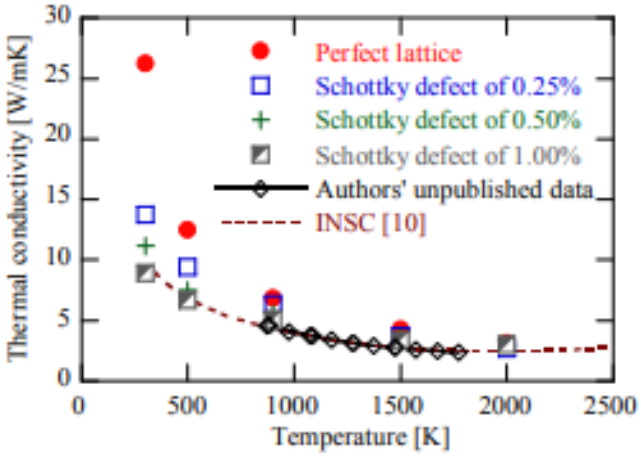

Figure 2. Thermal Conductivity of UO_2 (UCHIDA, SUNAOSHI, KATO, & KONASHI, 2011)

ii. Stresses and Cracking

During the early in-pile life of a fuel pellet, thermal expansion is not uniform through the pellet (Chiang, Faya, 1961). The center of the pellet is hotter than the edges, so it tends to expand more than the exterior of the pellet. This difference in expansion causes a tensile hoop stress at the pellet exterior and a compressive hoop stress in the center of the pellet. Ceramics such as UO_2 are stronger in compression than they are in tension, meaning that cracking is likely to occur from the exterior and propagate in. Cracks will continue to propagate inward until the local temperature drops the hoop stress below the cracking threshold.

b. Pellet Cladding Interaction

One impact of fuel cracking is its change in volume and shape, which can lead to pellet-cladding interaction (PCI). PCI is one cause of stress corrosion cracking of the fuel cladding. While the fuel can crack and still fulfill its basic function, cracked cladding results in fission product leaking into the coolant and effective failure of the fuel element. Clad cracking is caused by a mixture of mechanical and chemical effects (Olander, 2009).

Fuel pellets swell during irradiation due to the splitting of a fissile nucleus into two fission products, some of which are gaseous. When coupled with cracking caused by thermal stresses, the fuel pellet will swell in an “hourglass” shape as seen in figure 3.

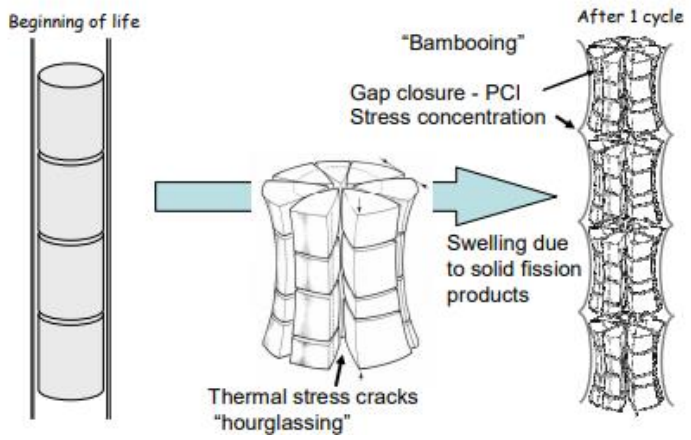

Figure 3. "Hourglassing" in Fuel Pellet (Olander, 2009)

This hourglass shape appears due to the conversion of plane strain near the midplane to plane stress near the upper and lower planes. When the pellet swells it can come into contact with the cladding and causes stress risers.

The chemical effects are caused in two ways. The first way is cladding embrittlement due to hydrogen precipitates that allow stresses to initiate cracking on the cladding outer diameter. The second is chemical effects from fission products interacting with the clad at mechanically stressed areas on the inner diameter of the clad. and cause stress corrosion cracking.

The combination of mechanical stress and chemical interactions can result in stress-corrosion-induced failures, including cracking such as that shown in figure 4.

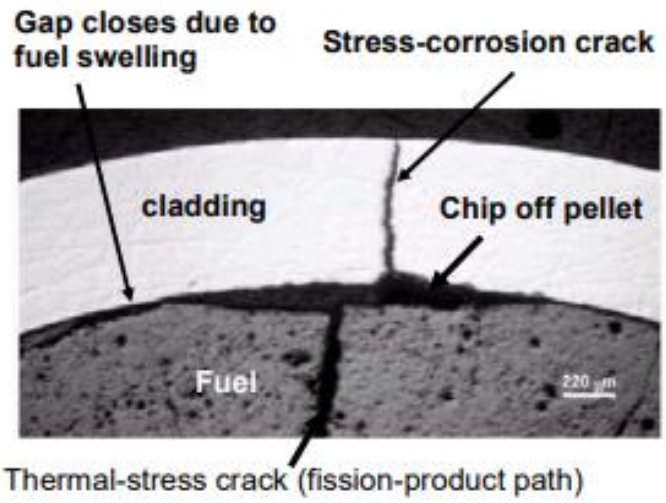

Figure 4. Cladding Cracking from Pellet-Cladding Interaction (Olander, 2009)

c. Bison Code

The Bison fuel performance code was used to model fuel pellet cracking for this thesis. The Bison code was developed at Idaho National Lab and is built on their Multi-physics Object Oriented Simulation Environment, or MOOSE, platform (Williamson, Hales, Novascone, Tonks, Gaston, Permann, Andrs, & Martineau 2012). MOOSE is a parallel finite element-based framework that is used to solve systems of coupled non-linear partial differential equations using the Jacobian-Free Newton Krylov or JFNK method. MOOSE is capable of using both 2D and 3D meshes. Bison is governed by fully-coupled partial differential equations for both energy and momentum conservation. The code has models that can be used to describe temperature and burnup dependent thermal properties, solid and gaseous fission product swelling, densification, thermal and irradiation creep, pellet fracture, and fission gas production, generation, and release.

d. Fracture Models

There are several approaches to modeling cracking, each with its unique advantages and disadvantages. The needs of a given project will dictate which approach is the best. The following is a description of two cracking model approaches that were used in this project.

i. Smeared Cracking

Smeared cracking was first used in 1968 for modeling prestressed concrete pressure vessels (Cerva, Chiumenti, 2006). The criteria for crack propagation comes directly from computational continuum mechanics based on failure criteria expressed in terms of stresses or strains. A crack develops when the principal stress surpasses the fracture stress (Burnett, & Schreyer, 2018). In order to calculate the stress needed to initiate cracking, a random number with a Weibull distribution is generated. This function is called VolumeWeightedWeibull. These models use a Weibull modulus of 12.0, a median cracking strength of 130 MPa, and a reference volume of 10^{-7} m^3.

This modeling method is simple and convenient to use, making it popular (Burnett, & Schreyer, 2018). However, there are some drawbacks. The method assumes that the crack orientation is related to the principal stress basis, which can lead to incorrect crack paths. Another drawback is dependence on mesh size. This mesh dependence means that the models are more accurate with a finer mesh, however with smaller mesh sizes the models use more memory and take longer to run.

ii. Extended Finite Element Method

The extended finite element method is a numerical method designed for treating discontinuities (Datta, 2013). It builds on the finite element method by extending the solution space to include differential equations and discontinuous functions. A major advantage of this over the finite element method is that the mesh does not need to be updated to track the crack path. However, this approach is more complicated than the smeared cracking approach.

Chapter 3. Experiments

a. Background

In light water reactors heat is produced through fission and moves through the plenum and cladding to the water coolant. The power in a light water reactor is changed slowly enough during ramping up that the fuel experiences quasi-steady-state thermal conditions at any point (Spencer et al., 2019). Typical radial temperature distributions in a light water reactor fuel pellet are shown in figure 5.

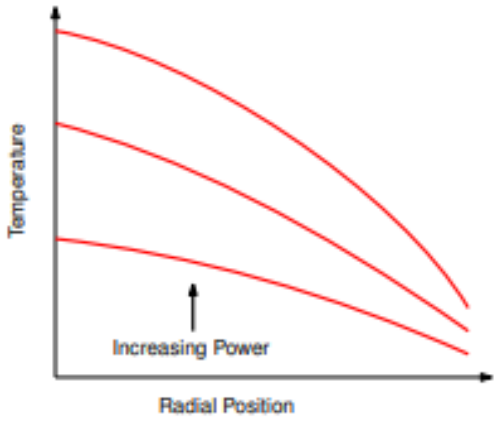

Figure 5. Radial Temperature Profile of a Fuel Pellet (Spencer et al., 2019)

It was important that the experiments in this project achieve this temperature profile as closely as possible so that they replicate a light water reactor environment. In addition, these experiments were designed to allow for observations of crack propagation with increasing power while limiting as many unrelated factors as possible. Each of the experimental designs, two out-of-pile and one in-pile, are described in more detail in this section.

b. Resistive Heating Experiment

The first out-of-pile experiment, which used resistive heating of the pellet, was performed at the University of South Carolina. At room temperature, UO_2 is electrically insulating; however,

as temperature increases the conductivity of UO_2 increases due to ionic conduction. This feature allows the UO_2 pellet to be volumetrically heated with resistive heating at sufficiently high temperatures. Electrodes were placed on opposite sides of the pellet and a current passed through the pellet. The geometry of the experiment leads to spatial variations in the heating that are different from what is desired, but it can be accounted for when modeling the experiment. Another challenge with this experiment design was achieving the pellet temperature necessary to reduce the electrical resistance enough to create the desired temperature profile. A molybdenum susceptor was used to achieve the temperature. The susceptor surrounds the pellet and inductively heats it until the electrical resistance falls below a threshold, beyond which a high current, low voltage direct current can create the desired temperature profile across the pellet. It was expected that cracking would develop along the plane between the electrodes.

This experiment allowed for real time observations of the cracking, as they initiate and propagate through the pellet. The real time imaging of the pellet in this experiment was accomplished using both optical and infa-red cameras. A beam-splitter was used to allow the cameras to be used simultaneously. While the optical camera was used to observe the cracks initiating and propagating, the infa-red camera was used to image the temperature gradient evolution. The temperature gradient data, in addition to cracking data, was useful for model development. After each experiment was run, images of the cracked pellets were collected using scanning electron microscopy or SEM, with the objective of correlating crack patterns and distributions with current levels. These images can also be compared to the final results of the models in order to validate the model.

There were three assumptions made in modeling this experiment. First, that the materials are homogeneous and isotropic; second, that there is a temperature dependent electrical

conductivity; and finally, that thermal and electrical conduction between electrodes and the fuel pellet is not significant (Yeh 2018). For joule heating the heat source is defined in W/m^3 by

$$\dot{Q} = \boldsymbol{J} * \boldsymbol{E} = J^2 \rho_e \quad (1)$$

where

$\mathbf{J} = \sigma\mathbf{E}$ is the current density in A/m^2

$\mathbf{E} = \nabla V$ is the electric field in volt/m

ρ_e is the electrical resistivity in Ωm

$\sigma = 1/\rho_e$ is the electric potential and

Laplace's equation $\nabla^2 V = 0$ applies when no unpaired electric charges exist.

This can be applied to the heat conduction equation for joule heating heat source

$$\rho C_p \frac{\partial T}{\partial t} - \nabla * (K \nabla T) - \dot{Q} = 0 \quad (2)$$

Momentum conservation at static equilibrium is given by

$$\nabla * \sigma = 0 \quad (3)$$

$$\sigma = E\varepsilon \quad (4)$$

$$\varepsilon = \nabla_s u + \alpha \Delta T \quad (5)$$

$$\nabla_s u = \frac{1}{2}(\nabla u + \nabla u^T) \quad (6)$$

where

σ is the Cauchy stress tensor,

α is the thermal expansion coefficient in 1/K,

$\nabla_s u$ is the strain rate tensor and

u are the displacements.

c. Quenching Experiment

Volumetrically heating ceramic fuel materials outside of a reactor is very difficult to accomplish. The resistive heating experiments already discussed required relatively complex equipment. The temperature quenching experiments conducted at Texas A&M University had the advantage of using a simpler design. The basic experimental procedure was to heat a fuel pellet in a high temperature bath and, when it reached the desired temperature, to remove it from that bath and quickly submerge it in a lower temperature bath. Cooling would occur at the outer edge first and produce the desired temperature profile across the pellet if the high and low temperature baths were sufficiently different. The equipment requirements were few: a hot bath, a cold bath, and some way to move the pellet between the two. Copper tubing was used to hold the pellet and to protect the pellet from the baths. Commonly available sized copper tubing was used, rather than manufacturing a copper holder to fit the pellet. Therefore, the pellet didn't fit perfectly in the copper tube and the gap between pellet and tube was larger than optimum for heat transfer. So, the pellet was pushed to one side of the copper tubing. Fittings on either end of the copper piping made it leak proof. The setup for this experiment can be seen in figure 6.

Figure 6. Quenching Experiment Apparatus (Spencer et al., 2019)

A molten salt bath was used to heat up the pellet. The pellet was slowly allowed to reach thermal equilibrium with the molten salt so that stresses large enough to induce cracking were not introduced during this phase of the experiment. After the pellet reached thermal equilibrium, it is removed and immediately dunked into a cold bath. The cold bath was kept cold enough to cause the thermal gradient needed to induce cracking in the pellet.

In modeling the quenching experiment, two assumptions were made. The first assumption is that the tensile strength of the UO_2 is 130 MPa and the second is that the materials are homogeneous and isotropic. This experiment is governed by the heat equation without a heat source (Yeh 2018). The heat equation without a heat source is

$$\rho C_p \frac{\partial T}{\partial t} - \nabla q = 0 \qquad (7)$$

where

ρ is the density in Kg/m^3

C_p is the specific heat in J/Kg*K

T is the temperature in K.

The heat flux is given by

$$q = k\nabla T \quad (8)$$

with initial condition

$$T(r,0) = T_i \quad (9)$$

and boundary condition

$$k\frac{\partial T}{\partial r}|_{r=R} = h(T_\infty - T_R) \quad (10)$$

where

k is the thermal conductivity of the material in W/m*K

T_i is the initial temperature in K

R is the cladding outer diameter

h is the convective heat transfer coefficient in W/m^2*K

T_∞ is the cold bath temperature and

T_R is the cladding outer surface temperature. The momentum conservation at static equilibrium is the same the quenching experiment as the resistive heating experiment.

To account for randomness in the material, a random number generator using a Weibull distribution was used to calculate the cracking strength. For this calculation, a reference volume and Weibull modulus must be provided. For the 2D models, the reference volume is 10^{-7} m^3 since setting this value equal to the nominal element volume in the mesh gives a tensile strength equal to the nominal value that is specified. This allows the tensile strength to be tuned to a published value and should make the results relatively independent of the mesh size. For the 3D models a reference volume of 10^{-9} m^3 was used, and a Weibull modulus of 12 is used for both cases.

d. Transient Testing Reactor

Conditions of the experiment performed in Idaho National Laboratory's transient reactor test facility, or TREAT, is the most representative of a light water reactor environment. TREAT has characteristics that make it uniquely capable of running this experiment. First is the fact that the transient produced by the reactor can be shaped as desired as long as it fits inside of certain limits. This feature allows each experiment to have its own irradiation history. Next, TREAT is not cooled by water, which allows easier installation of monitoring instruments and easier use during the experiment compared to a water-cooled reactor. While absence of water is an advantage of the TREAT reactor, it was still necessary to replace the heat removal role that water plays in an LWR. To remove heat from the pellets during the experiments, a stainless-steel heat sink was used. The experimental assembly was a dry-in-pile fracture test, or DRIFT. The DRIFT was place inside a separate effects test holder, or SETH, which was placed inside a minimal activation retrievable capsule holder, or MARCH, which was placed into the TREAT reactor. A coil heater, wrapped around the DRIFT test fixture, was used to control the starting temperature, but not for heating during the actual experiment.

Due to the transient nature of the TREAT reactor, the desired temperature profile can be maintained only for an instant. This phenomenon is due in part to the fact that the heat flux from the fuel decreases with time. The heat sink starts at a low temperature but as the experiment runs the heat sink steadily heats up, causing heat flux from the pellet to decrease as the experiment continues.

The main goal of this experiment is to get "screenshots" of fuel crack progression and to use these images to validate cracking patterns produced by the Bison model. The experiments conducted to replicate fuel at various power levels and different operational histories. Five

experiments, with power levels ranging from 5 kw/m to 25ks/m, were conducted. Each experiment was ramped to power until the temperature profile replicated an LWR temperature profile and then the reactor was shut off. Each experiment contained several pellets to give a good sample of the cracking at each power level and history. Several temperature sensors were placed around the apparatus to allow for monitoring of the fuel pellets in the reactor.

The heat generation rate produced by fission is given by

$$\dot{Q} = G * N * \sigma_f * \Phi * V_f \quad (11)$$

where

$\dot{Q}$ is the heat generation rate,

G is the energy released per fission,

N is the number of fissionable fuel nuclei per unit volume,

σ_f is the microscopic fission cross section,

V_f is the volume of the fuel,

And Φ is the neutron flux (U.S. Department of Energy, 1992).

Chapter 4. Results and Discussion

The majority of original work done for this thesis was in support of the temperature quenching experiments conducted at Texas A&M. The results of this work are summarized in Section 4a. Some additional modeling work was conducted to support the TREAT experiments and is presented in section 4b.

a. Quenching

i. Heat Transfer Coefficient

In order to model the quenching experiments. it was necessary to determine the coefficient of heat transfer between the copper tubing and the cold bath. To accomplish this, a copper slug was instrumented with thermocouples through its centerline and beside it, and then heated and quenched in the same way planned for the pellets. The cold bath temperature was monitored with a thermocouple and a thermocouple also was placed in the hot bath The experiment setup including the copper slug and center and outside thermocouples can be seen in figure 7.

Figure 7. Copper Slug with Two Thermocouples

The copper slug was heated in a molten salt bath kept at approximately 973 K for about 145 seconds. When the centerline temperature of the slug reached 952 K, it was removed from the molten salt bath and immediately placed in a 50/50 mix of water and ethylene glycol kept at 263 K. At 140 seconds, the centerline temperature of the slug reached 273 K. During the slug cooling process, temperatures were recorded at half second intervals.

After this experiment was conducted, a model of the slug cooling was developed in MOOSE. This model used a time dependent heat transfer coefficient function called Convective flux function. This function allowed for adjustment of the heat transfer coefficient at each time step so that the modeled temperature would match the experimental temperature. Output from this model is seen in figure 8.

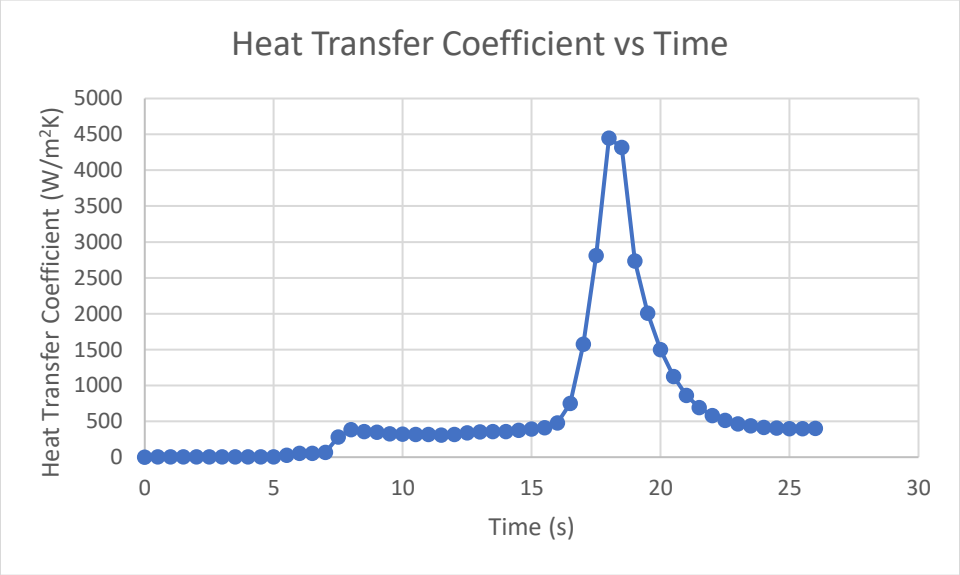

Figure 8. Heat Transfer Coefficient for Copper slug

As can be seen from the plot, early in the time the slug spent in the cooling bath, when the copper slug is very hot, the heat transfer is very low. This behavior is likely due to a vapor gap forming between the water ethylene glycol mix and the copper slug. This gap occurs because the copper slug is so hot that the cold bath will immediately boil when the slug is put in it. As the

copper slug cools and the cold bath liquid can make better contact with the copper slug, the heat transfer coefficient increases. Eventually the slug has cooled enough that the heat transfer coefficient decreases, as the temperature difference between the copper slug and cold bath decreases.

1. Temperature Dependent Function

The cooling profile for the copper slug experiment was useful for informing the ceramic pellet cooling models; however, manually changing the heat transfer coefficient for each time step was a tedious and inefficient process. To increase the efficiency of coefficient calculation in the model, a temperature dependent function was developed. This allowed the same .csv file, with the heat transfer coefficient, to be used for all of the experiment models.

This was very helpful in reducing model run time as well as allowing these results to be applied to a different experiment. By creating this function, the results from a solid copper slug being quenched could be applied to the hollow copper tube that is used the quenching experiment.

ii. Cold Bath Determination

Another important parameter of the quenching experiments was the composition of the cold bath. Two compositions were considered. The first was a 50/50 mix of water and ethylene glycol. The ethylene glycol allowed the water to get to a lower temperature without freezing. This mixture could be cooled to 263 K without freezing. The other composition considered was a simple ice bath. Initially it was believed that the mixture of water and ethylene glycol was going to be the better option for the cold bath given that it was able to get colder without freezing.

In determining which material was truly the better cold bath option, the heat transfer coefficient was the main consideration. This meant going through the same process described for determining the heat transfer coefficient for copper. Copper slugs were heated in molten salt then

quenched in a cold bath. Thermocouples measured the temperature in the hot bath, cold bath, the centerline of the slug and just outside of the slug every half second. Models of each experiment developed using the time dependent heat transfer coefficient function and the heat transfer coefficient was adjusted in order to make the temperatures match.

There were three experiments conducted for comparison of the cold bath material. One used the mixture of water and ethylene glycol and two used an ice bath, one with a short copper slug and one with a longer slug. While it was logical to use the same process to find the heat transfer coefficient, it was not possible to compare the results in terms of time given that they were heated to different temperatures before cooling and quenched for different amounts of time. Instead, the heat transfer coefficients were compared relative to temperature, which was possible because there were large overlaps in temperature ranges for the three experiments. The results were plotted together and compared to a reference line that was found in the paper "Characterization of Heat Transfer during Quenching" (Hernandez-Morales, 2013). The results from this exercise are shown in figure 9.

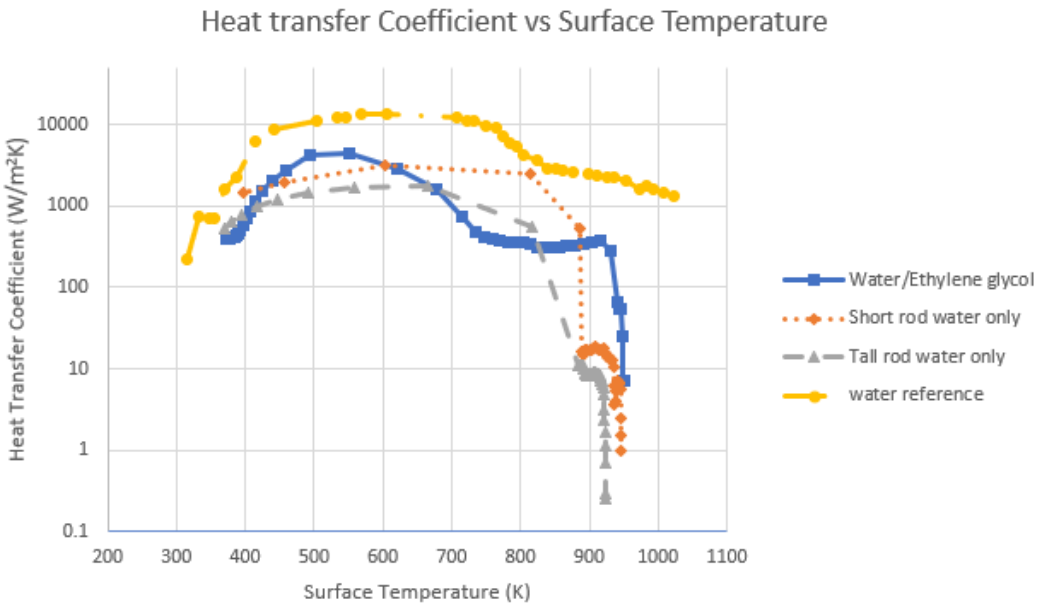

Figure 9. Cold Bath Heat Transfer Coefficient Comparison

As shown in Figure 9 the heat transfer coefficients vary similarly with temperature and there is no clearly superior candidate. Because there was no advantage relative to the heat transfer coefficient, the simpler cold bath composition was chosen. This choice was also advantageous because ethylene glycol burns at the temperatures being reached in the UO2 experiments.

iii. Minimum Temperature for Cracking

Experimenters were interested in knowing the minimum hot temperature of the pellet that would result in cracking, because heating was time consuming. The minimum temperature was estimated using the models that were developed for this experiment. Because it was initially believed that 950 K was the highest temperature achievable in these experiments, that value was used as the starting point for this modeling exercise. The initial temperature of the pellet set to 950 K, the cold bath set to 273 K, and the model was run for 30 seconds. As expected, model output indicated severe cracking in the pellet, as shown in Figure 10.

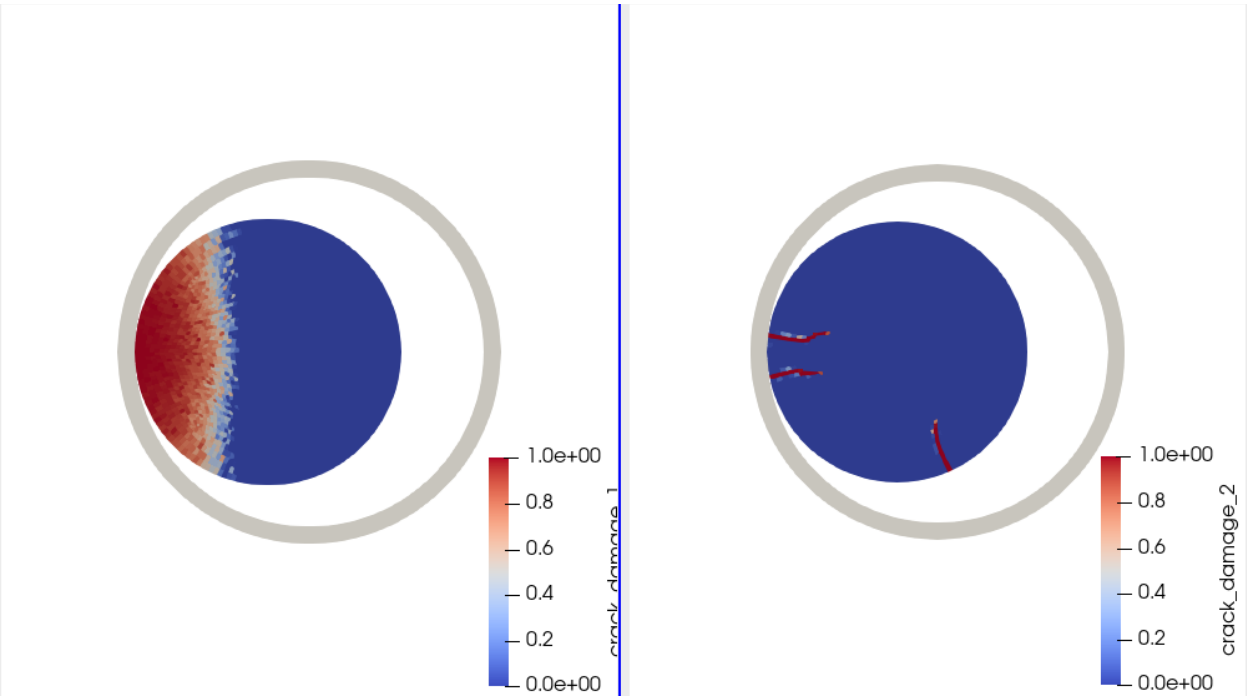

Figure 10. Predicted Axial (Left) and Radial (Right) Cracking at 950 K

The images in Figure 10 show axial cracking through roughly one third the pellet and there are also multiple radial cracks. For subsequent model runs, the initial temperature of the pellet was lowered by intervals of 50 K. The amount of cracking dropped as the initial temperature was lowered. At 750 K initial temperature, there was a significant decrease in the amount of cracking, as shown in figure 11.

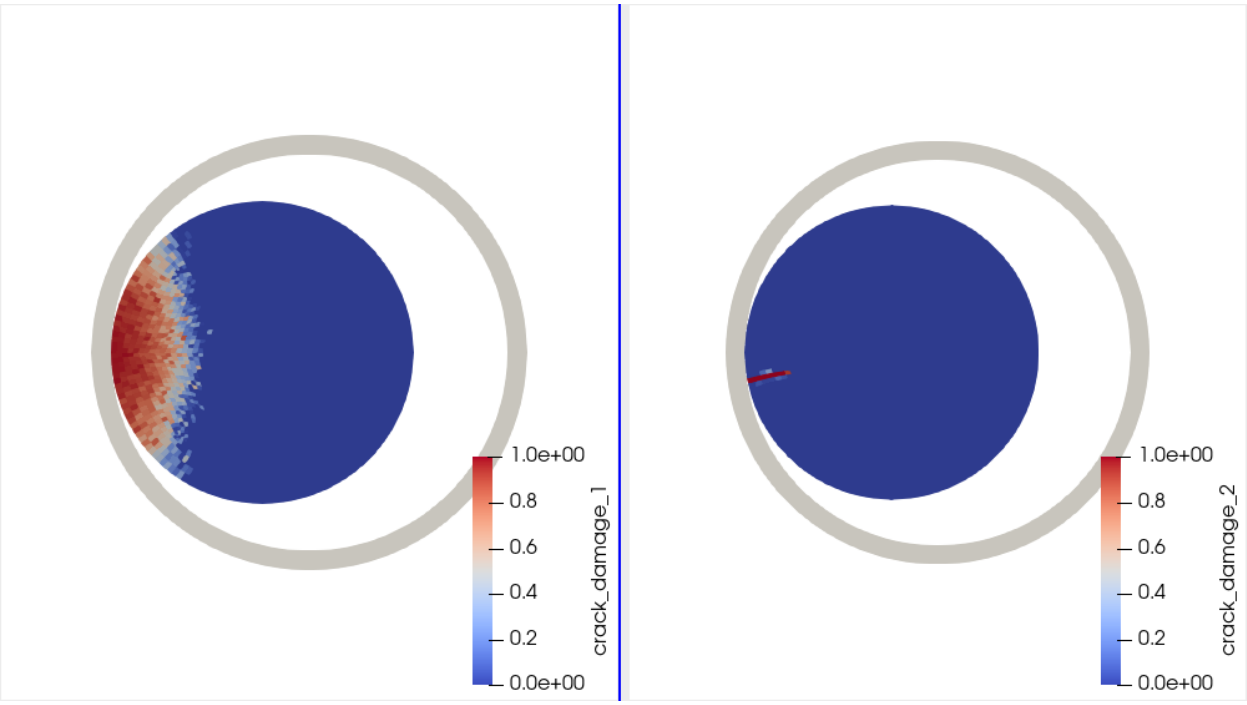

Figure 11. Predicted Axial (Left) and Radial (Right) Cracking at 750 K

Both the axial and the radial cracks in this model were significantly lower than at 50-degree higher initial temperature. Below 750 K initial temperature, there was no radial cracking. At 450 K initial temperature, there was very little axial cracking (Figure 12). Below 450 K, neither radial nor axial cracking occurred.

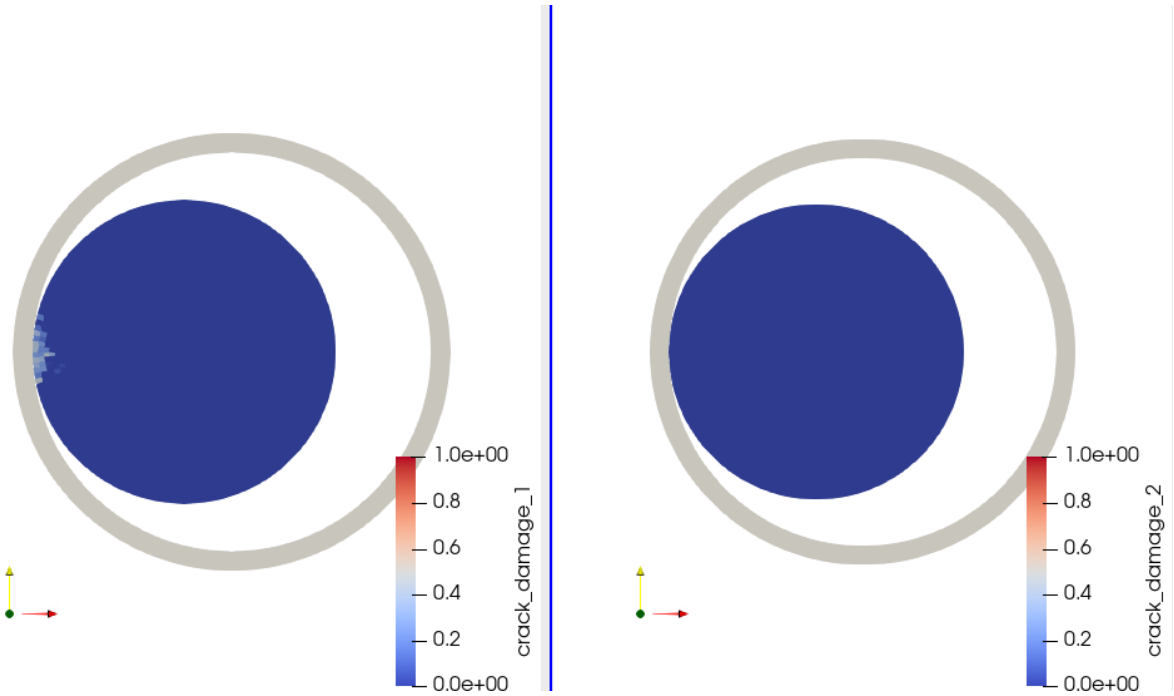

Figure 12. Predicted Axial (Left) and Radial (Right) Cracking at 450 K

450 K was significantly lower than the predicted minimum temperature to cause cracking. This result implied that experiments could be conducted in less time than originally thought.

iv. Time Step Size Determination

The cracking models have some dependence on the size of the time step used. Smaller time steps show more accurate results than larger ones, due to the lag in calculating the cracking in these models. This lagging allows larger error to occur with larger time steps. For this project it was important to balance the accuracy of the results with the time it takes to run each model. So, it was important to find the ideal time step size. To determine the time step optimum size, the model was run with varying time steps and the cracking from each run was compared. It was decided to start with half second intervals because that was the interval at which temperature was record during the experiments. The time intervals were then decreased and rerun until there was

little increase in accuracy with subsequent step size reduction and the total run time was reasonable. To determine when these solutions had converged the integrated crack damage 1, which was the axial cracking, was plotted against the time for every trial. Results are shown in figure 13.

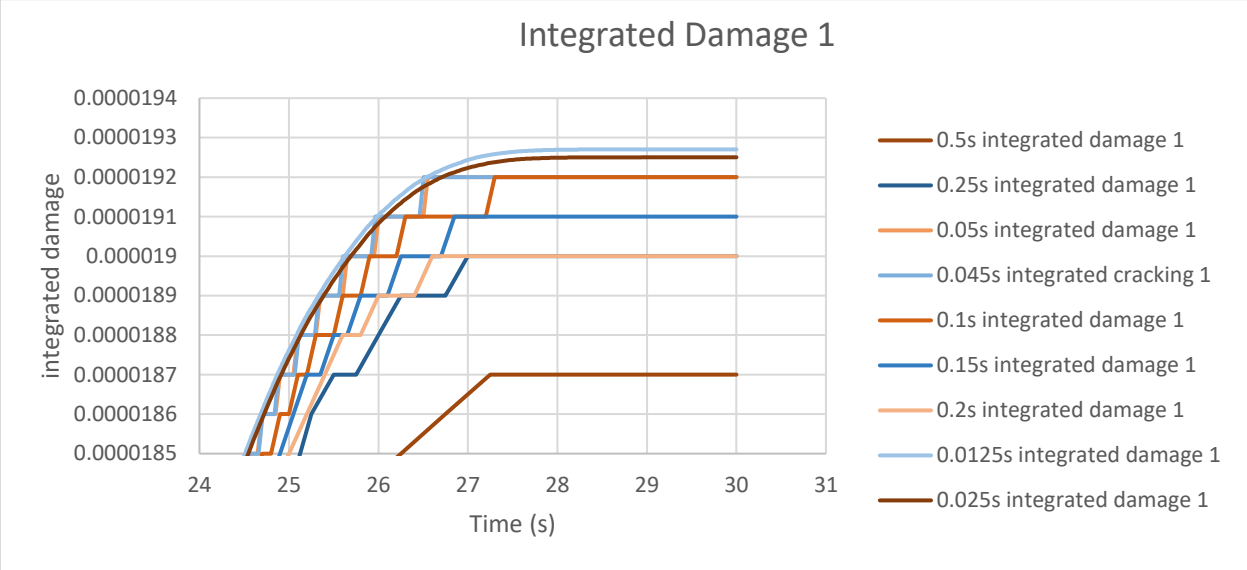

Figure 13.Damage at Varying Time Step Sizes

In Figure 13, the convergence of the results can be seen. There is a large difference between the first trial of half second time steps and quarter second time steps. These models were run with a relatively low temperature in comparison to the experiments. So, error in the results would get larger as the model temperature gets larger. As the time steps interval decreases, the model output becomes more similar. The difference between model output for time step intervals at 0.025 seconds and 0.0125 seconds is insignificant. Therefore, the longer time step interval of 0.025 seconds was chosen to increase efficiency in run time.

As shown in figure 14, no matter the time step size no cracking appeared in the models before 16 seconds. This appeared to be true no matter what the temperature as well. This makes

sense when looking at the heat transfer coefficient vs time plot in figure 8, the heat transfer coefficient starts to spike around 16 seconds, indicating the time it took to cause the required stresses and crack the pellet. Because there was no cracking during the first 16 seconds, a time stepper function was used to skip quickly over this time period to decrease model run time. Rather than running the entire 30 second model at 0.025 second intervals, the first 16 seconds were run at half second intervals.

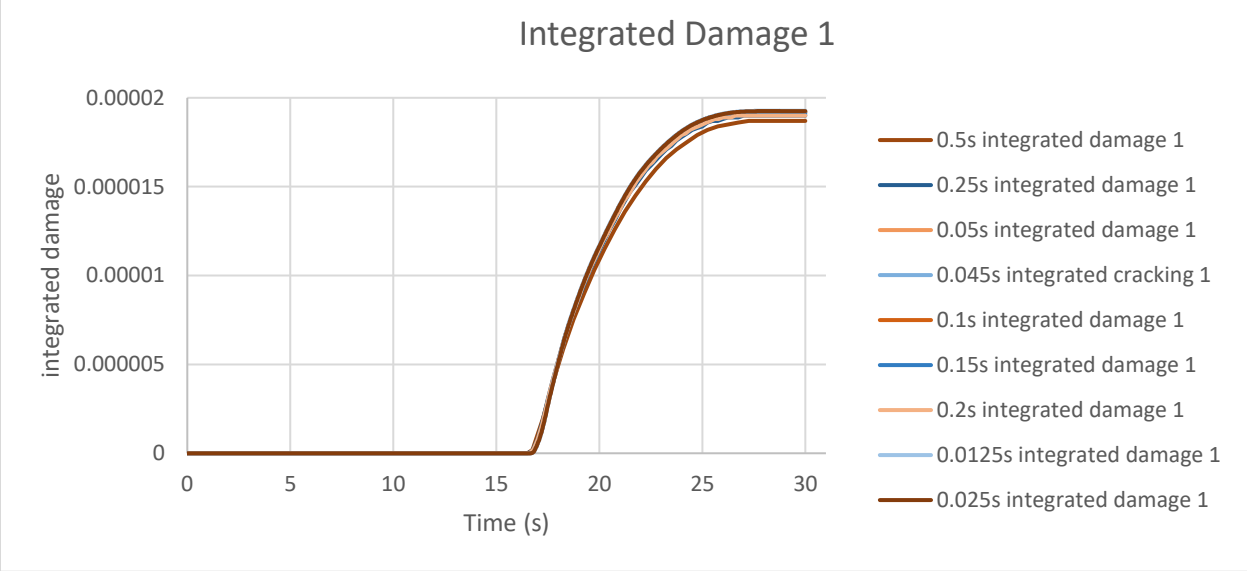

Figure 14. Full Plot of Crack Damage vs Time

v. Model Run for Each Experiment

After the experiments were conducted, a model was run for each experimental trial. Experimenters provided trial parameters, including pellet dimensions, copper tubing dimensions, and temperature readings for the hot bath, cold bath pellet centerline and just outside of the pellet. Meshes for every pellet and cladding pair were made and the input file was edited to be run for every experiment. Modeling these experiments was complicated by failing thermocouples and varying experimental designs. The environment that the thermocouples were subjected to was very harsh and caused several to fail. The result was temperature data that varied wildly between time

steps in a non-physical manner, making it difficult to discern true temperature. This phenomenon coupled with changing experimental design made the modeling more difficult. As experiments were conducted it obvious what scenarios worked well and what did not. For example, in some experiments copper foil was used on one side of the pellet to push the pellet to the side of the copper tube, in other experiments the copper foil was used on both sides of the pellet. and in some experiments an insulating material was used on one side of the pellet. To simplify the modeling amidst the varying experimental parameters, it was assumed that in all experiments the pellet was held to one side in direct contact with the copper tubing and the tube was filled with helium. Helium is used in this model because it is the most conductive gas and is also inert making it ideal for experiments like this.

The next step in the process was to compare model prediction of pellet cracking with experimental results. This was a challenging exercise, beginning with the question of what to compare (crack length, crack volume, crack penetration, etc.). Several approaches were considered. One option was to measure the length of every crack and sum the values to a total crack length. Another option was to measure the total cracking length as well as the depth of the deepest crack then comparing relative to both values. Yet another option was to measure each crack and compare the number of cracks by severity. A histogram could be created to compare the number of cracks at each determined length for the modeled and experimental results.

1. U6-72

Pellet U6-72 was the second pellet to be quenched and the first pellet that was successfully cracked through quenching. The pellet was 10.33 mm tall and had a diameter of 11.45 mm. It was placed inside a copper tube (177.8 mm tall, inner diameter 14.5 mm, outer diameter of 15.9 mm.) To keep this pellet against the wall of the copper tubing. 19.93 mm of copper foil was folded 32

times and placed on one side of the pellet. This pellet was heated to 1025 K and quenched in a 50/50 mix of water and ethylene glycol that was kept at 263 K. The results of this experiment were potentially compromised by a couple of things. First, during the experiment, liquid from the bath(s) leaked into the tubing, which may have impacted the amount of cracking that occurred. It is also thought that the amount of epoxy that was used to hold the pellet in place could have affected the amount of cracking that occurred.

This pellet was cut into 3 sections for crack imaging. A diagram of the sectioning of this pellet is shown in figure 15. A fair amount of cracking occurred, as can be seen in figures 16 through 22.

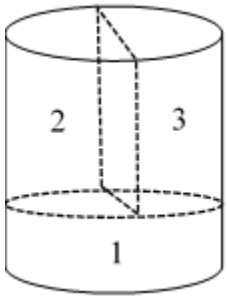

Figure 15. Pellet U6-72 Imaging Diagram (Ortega, Yee, 2021)

Figures 16-18 show section 1 of pellet U6-72. From this view little cracking can be seen. It is difficult to see any cracking in the optical image in figure 16 but it can be seen well in the SEM images in figures 17 and 18.

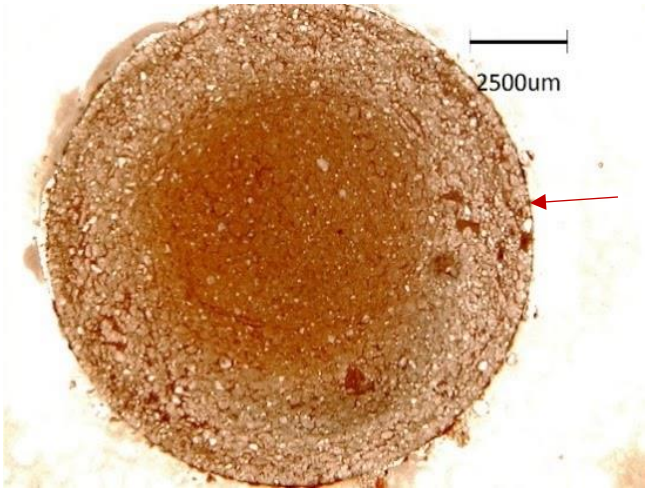

Figure 16. Optical Image of Section 1 of Pellet U6-72 (Ortega, Yee, 2021)

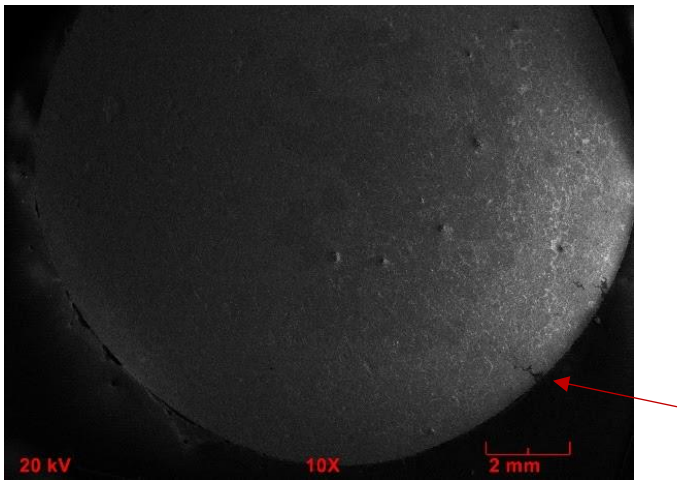

Figure 17. SEM Image of Section 1 of Pellet U6-72 (Ortega, Yee, 2021)

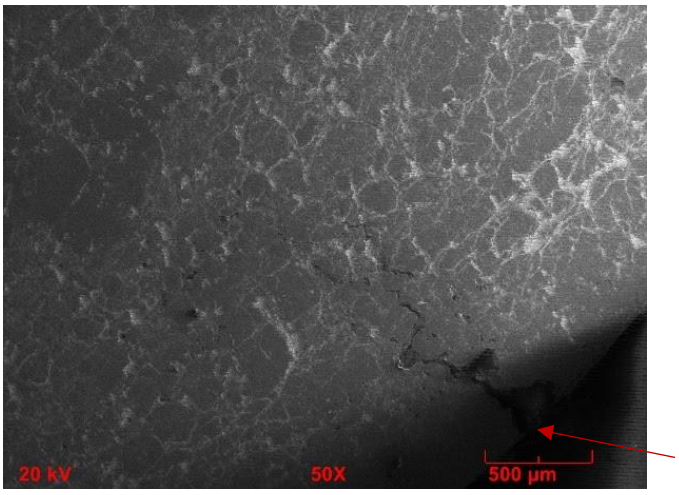

Figure 18. Zoomed in SEM images of section 1 of Pellet U6-72 (Ortega, Yee, 2021)

Figures 19 and 20 show images of section 2. This section experienced extensive cracking. The optical image shows severe cracking but there are a few cracks that are clearer on the SEM images.

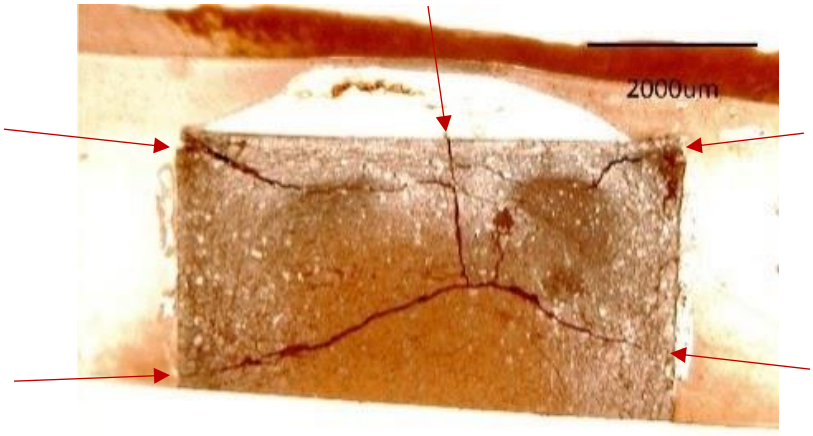

Figure 19. Optical Image of Section 2 of U6-72 (Ortega, Yee, 2021)

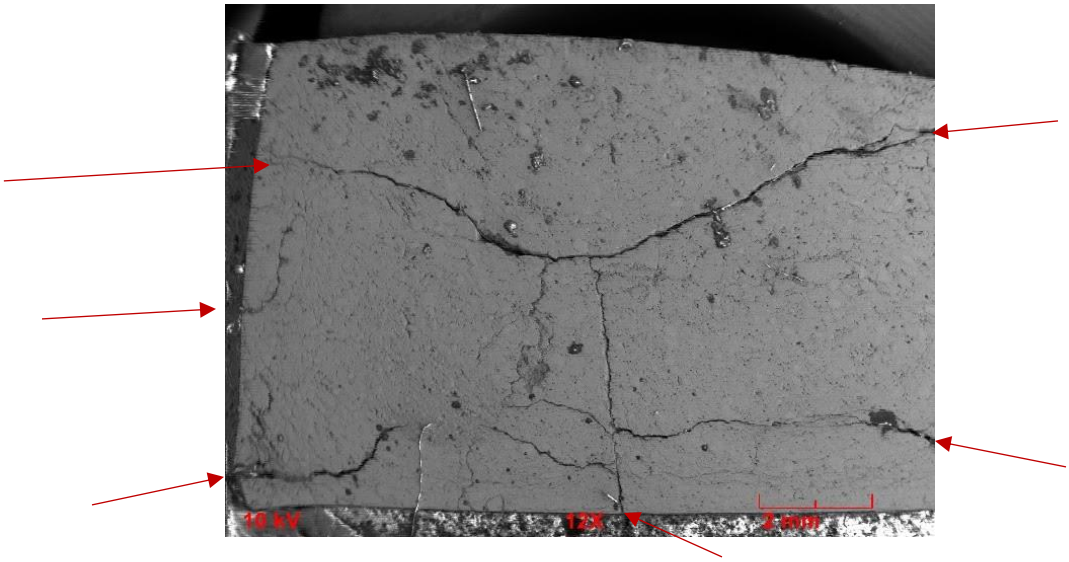

Figure 20. SEM Image of Section 2 of U6-72 (Ortega, Yee, 2021)

Section 3 shows cracking very similar to that seen in section two of this pellet. This similarity is consistent with the method of pellet cutting and the relationship of the two sections to

each other in the pellet. Much like section two, the optical image for section three shows a fair amount of cracking but there are some cracks that are easier to see in the SEM image.

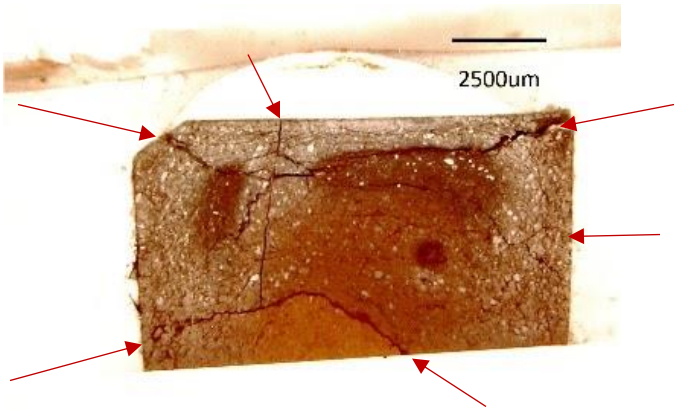

Figure 21. Optical Image of section 3 of Pellet U6-72 (Ortega, Yee, 2021)

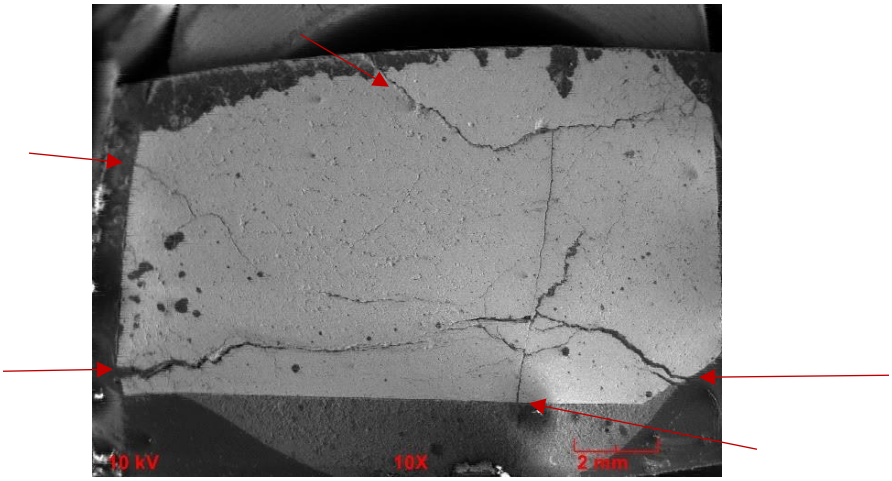

Figure 22. SEM Image of Section 3 of Pellet U6-72 (Ortega, Yee, 2021)

Both the 2D and the 3D models for this pellet predict extensive cracking as well. The predicted axial cracking is shown in figure 23 and the predicted radial cracking of the pellet is shown in figure 24.

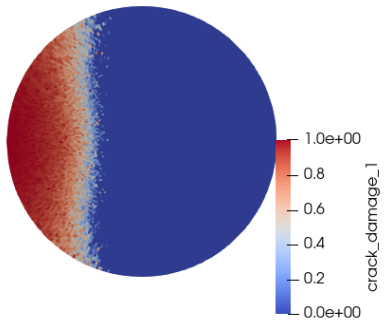

Figure 23. Predicted Axial Cracking of U6-72

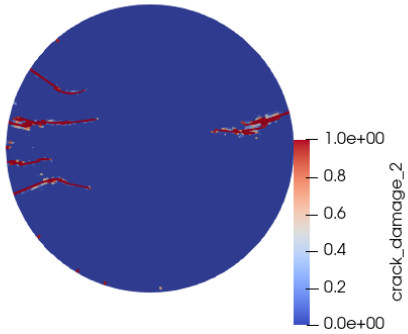

Figure 24. Predicted Radial Cracking of U6-72

To compare the modeled predictions with the experimental results the total visible length of cracking in each was compared. For this experiment the total cracking length was 1.3 cm. The 2D model of the experiment predicted only 0.9 cm, roughly 67% of the cracking that occurred in the experiment. While the 2D model was well short of predicting the actual cracking that occurred, the 3D model did better. The results of the 3D model are shown in figures 25 through 27.

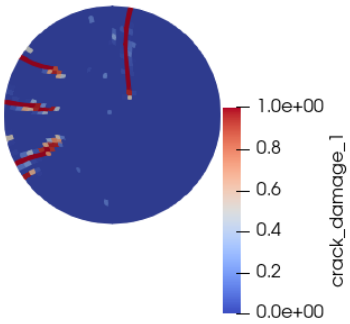

Figure 25. Top of the 3D Model of Pellet U6-72

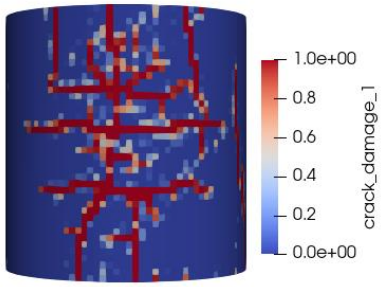

Figure 26. Side of the 3D Model of Pellet U6-72

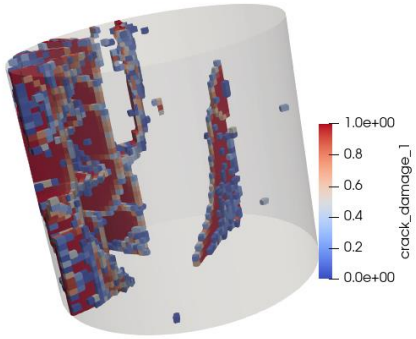

Figure 27. Filtered Cracking in 3D model of Pellet U6-72

The 3D model predicts about 1.4 cm of total crack length, which is actually slightly more than what actually occurred. This model predicted roughly 106% of the cracking that occurred in the experiment.

2. U6-71B

Pellet U6-71B was 9.77 mm tall and had a diameter of 11.53 mm. It was put in a copper tube that was 177.8 mm tall with an inner diameter of 14.5 mm and an outer diameter of 15.9 mm. The pellet was pushed against the side of the copper tubing using insulating material. The pellet-tube assembly was heated to 913 K and quenched in a 50/50 mix of water and ethylene glycol that was kept at 263 K. The modeling of this experiment was complicated by the fact that thermocouples failed. As such, the reliability of the data in question.

Significant cracking occurred in the pellet; however less post-cracking examination of the pellet was conducted. This pellet was cut into only two sections, the top half is section A and the bottom half is section B. There is a single SEM image but several optical images for this pellet. Significant cracking occurs in the pellet axial center, which can be seen in the optical image in figure 28 or the SEM image in figure 29.

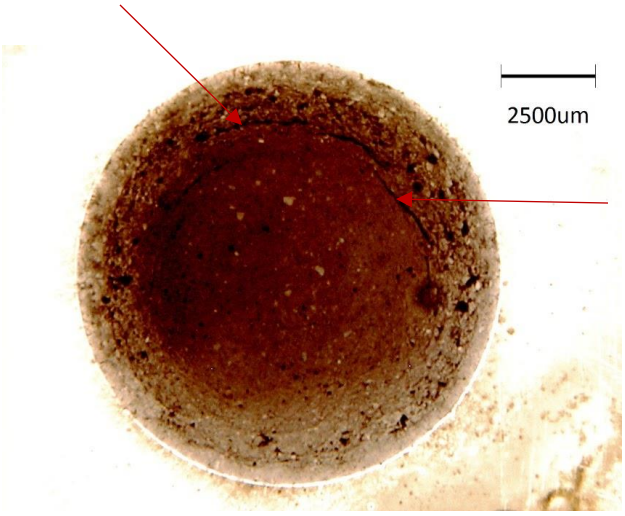

Figure 28. Optical Image of the Center of U6-71B (Ortega, Yee, 2021)

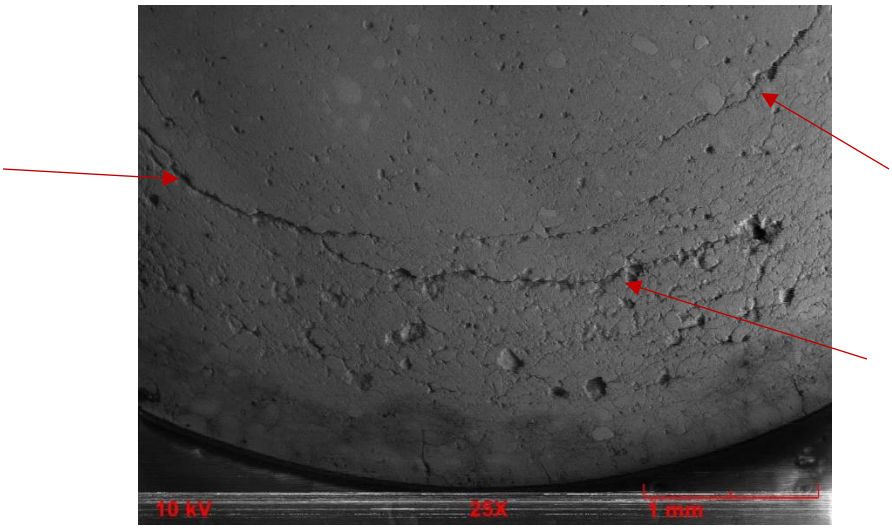

Figure 29. Zoomed in SEM Image of U6-71B (Ortega, Yee, 2021)

These images show a fair amount of cracking around the edges of the pellet. The cracks on the bottom of the pellet, as shown in figure 30, appear to be fairly shallow but show up in a similar pattern to what is seen in the center of the pellet. These shallow cracks also appear on the side of the pellet as can be seen in figure 31.

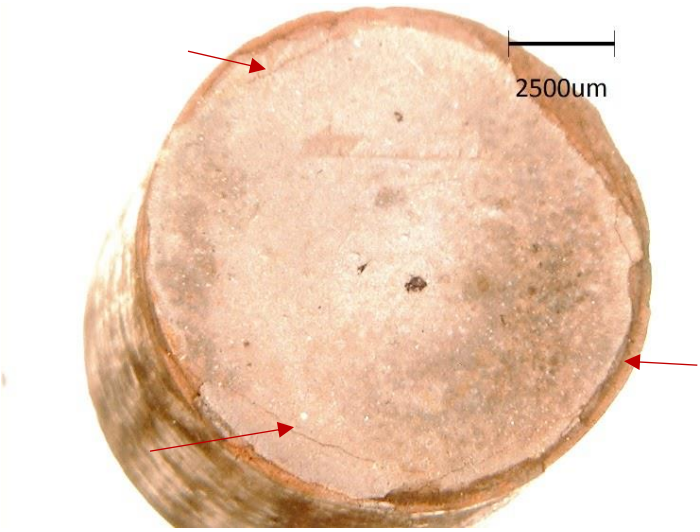

Figure 30. Bottom of Pellet U6-71B (Ortega, Yee, 2021)

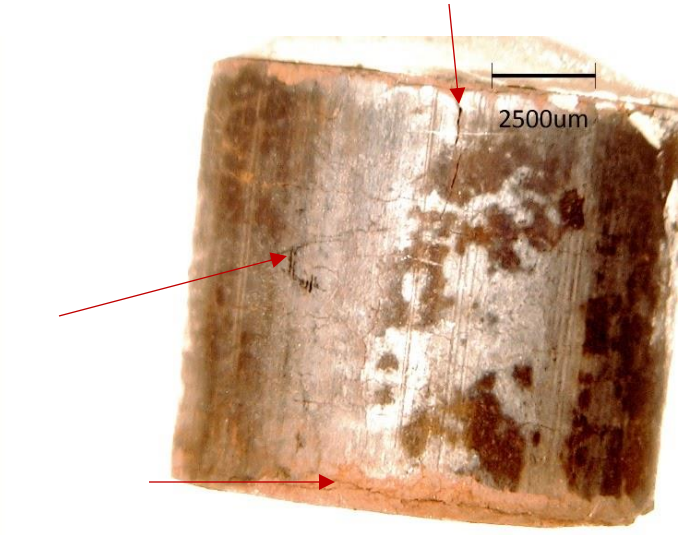

Figure 31. Side of Pellet U6-71B (Ortega, Yee, 2021)

The cracking on both the side and the bottom of the pellet are difficult to see, making them difficult to measure. However, measurements were made and the total length of cracking added up to 3.6 cm.

The models of this experiment also predicted significant cracking. The 2D model output, shown in figures 32 and 33, show several large cracks, including axial cracks similar to that predicted for pellet U6-72. The pellets differ in the amount of radial cracking. The 2D model predicted about 2.9 cm of total cracking length, which is about 80% of the cracking that actually occurred.

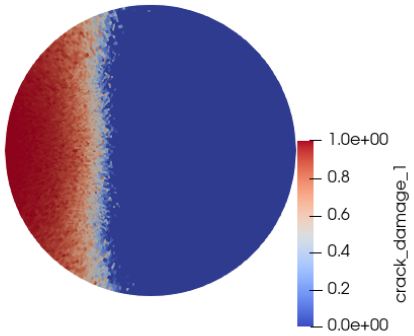

Figure 32. Predicted Axial Cracking of Pellet U6-71B

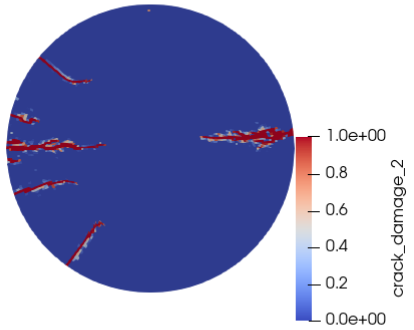

Figure 33. Predicted Radial Cracking of Pellet U6-71B

As before, the 3D model predicts slightly more cracking than the 2D, as is shown in figure 34. This model predicted about 3.2 cm of total crack length which is 90 % of the cracking that occurred.

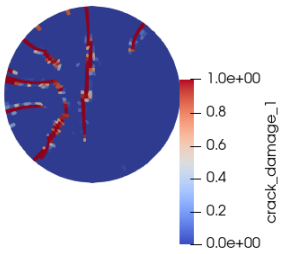

Figure 34. Predicted Cracking on Top of the 3D Model

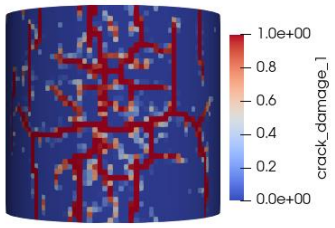

Figure 35. Predicted Cracking on the Side of the 3D Model

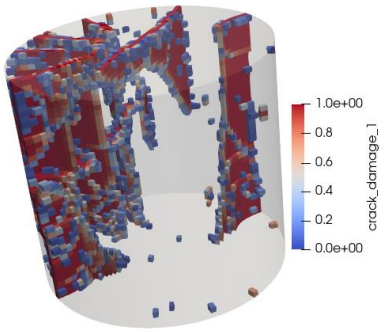

Figure 36. Filtered Cracking in the 3D Model

3. U6-40

Pellet U6-40 was 9.45 mm tall and had a diameter of 11.25 mm. It was put in a copper tube that was 143.6 mm tall, it had an inner diameter of 14.0 mm and an outer diameter of 15.9 mm. 762 mm of copper foil was folded into 12 layers that, shaped into a U and placed around the pellet to make contact on two sides of the pellet. The pellet-tube assembly was heated to 940 K and quenched in a 50/50 mix of water and ethylene glycol that was kept at 262 K. Much like U6-71B the data gathered in this experiment was compromised by failing thermocouples. This pellet was cut into 3 sections, as illustrated in figure 37, for imaging.

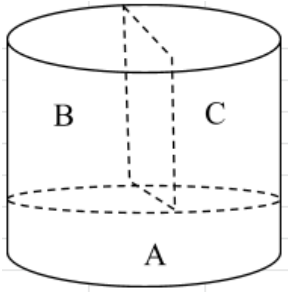

Figure 37. U6-40 Imaging Diagram (Ortega, Yee, 2021)

This pellet had less cracking than previous experiments as seen in figure 38. On section A there are a couple small cracks that grow close together and almost look like a single crack in the optical image. The SEM images allow differentiation of the two cracks.

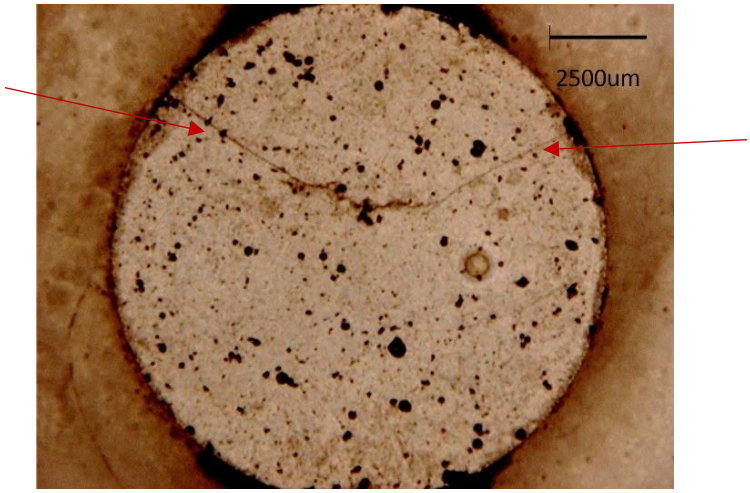

Figure 38. Optical Image of Section A of U6-40 (Ortega, Yee, 2021)

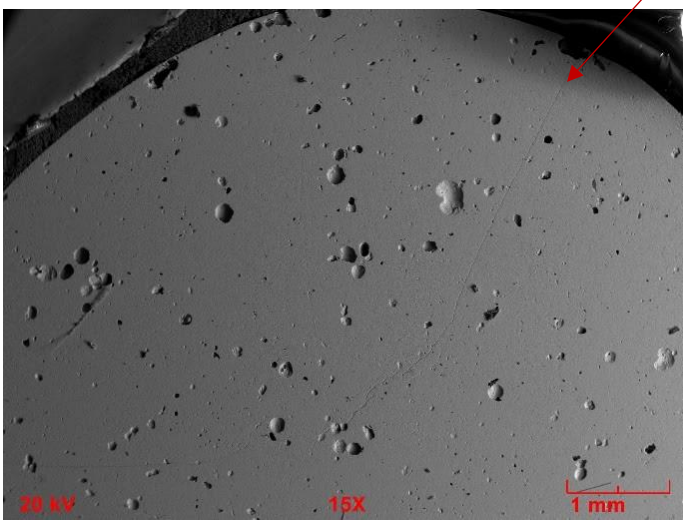

Figure 39. Zoomed in on First Crack of SEM Image of Section A of U6-40 (Ortega, Yee, 2021)

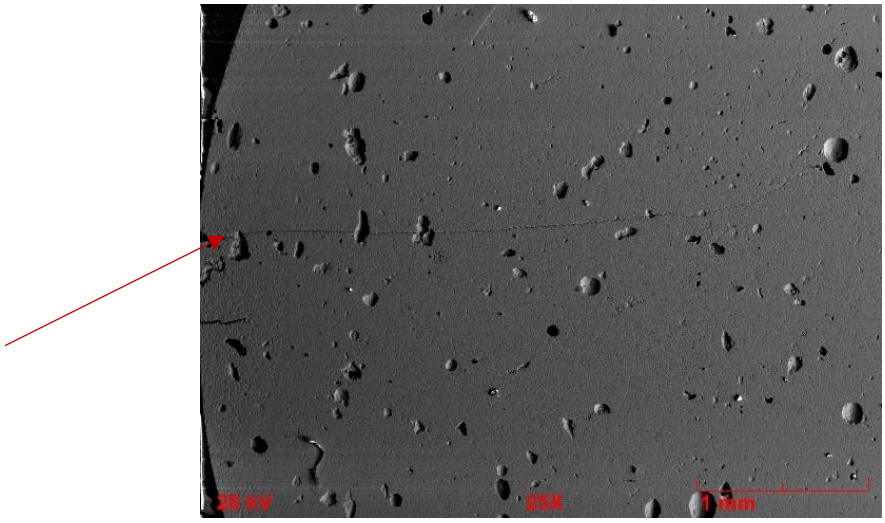

Figure 40. Zoomed in on Second Crack of SEM image of Section A of U6-40 (Ortega, Yee, 2021)

It is easier to differentiate the cracks in the optical image of section B than in section A but the SEM shows more cracks than can be seen in the optical images. The cracks in this section are still fairly small but they are easier to differentiate.

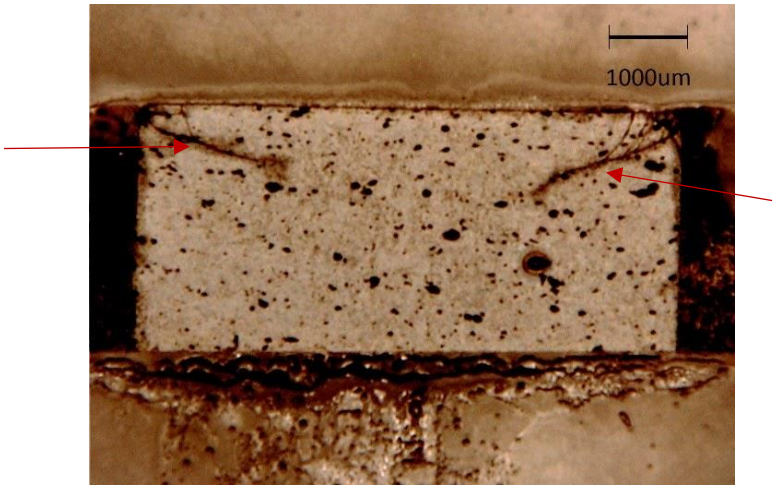

Figure 41. Optical Image of Section B of U6-40 (Ortega, Yee, 2021)

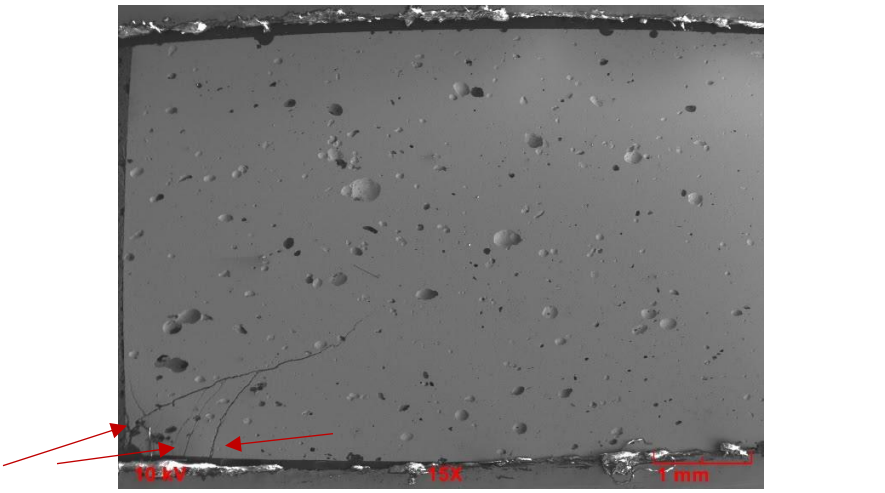

Figure 42. SEM Image of Crack 1 in Section B of U6-40 (Ortega, Yee, 2021)

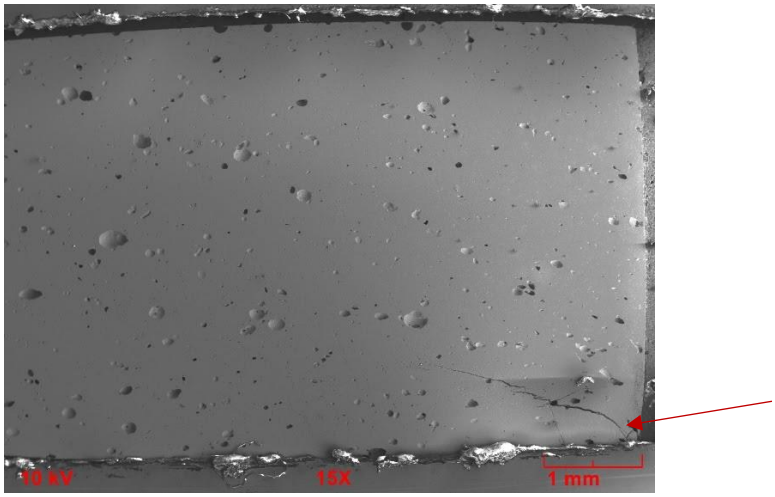

Figure 43. SEM Image of Crack 2 in Section B of U6-40 (Ortega, Yee, 2021)

These images show little cracking in the pellet in this experiment, which is comparable to the model predictions (in Figures 44 through 48).

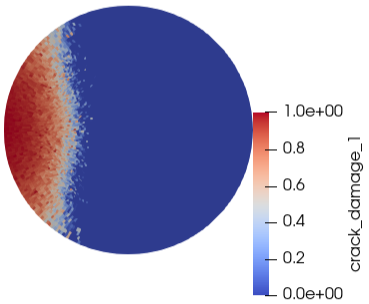

Figure 44. Predicted Axial Cracking of U6-40

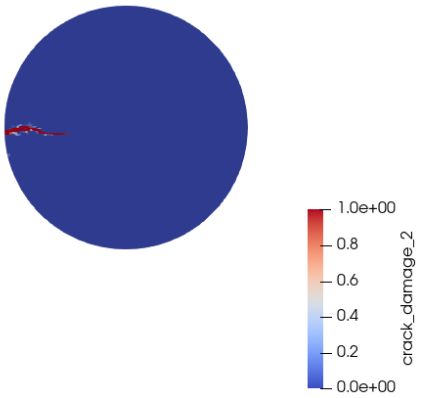

Figure 45. Predicted Radial Cracking of U6-40

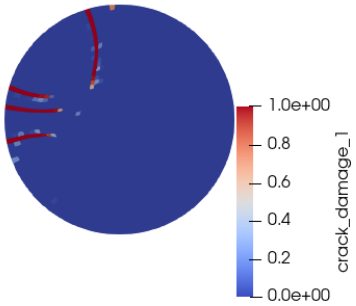

Figure 46. Predicted cracking on Top of 3D Model of U6-40

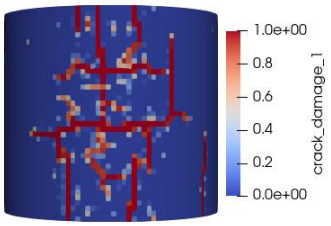

Figure 47. Predicted Cracking on Side of 3D Model of U6-40

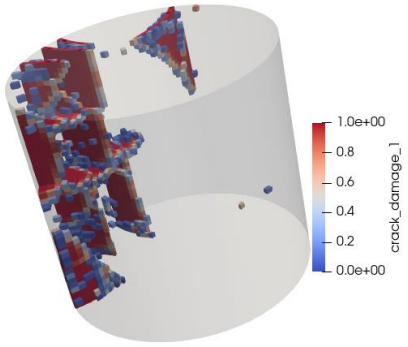

Figure 48. Filtered Cracking Predicted by 3D Model of U6-40

The total cracking length measured was about 1.05 cm, compared to the 2D model predicted a total cracking length of 0.8 cm. The 2D model is only accounting for roughly 76% of the cracking that actually occurred on this pellet. The 3D model predicted a total crack length of 1.14 cm of cracking which is actually slightly more than actually occurred, 108%.

4. U4-53C

Pellet U4-53C was 9.43 mm tall and had a diameter of 11.05 mm. This pellet was placed in a copper tube that was 180 mm tall with an inner diameter of 14.5 mm and an outer diameter of 15.9 mm. Insulating material was used to push the pellet to one side of the copper tube. The pellet-tube assembly was heated to 935 K and quenched in a 50/50 mix of water and ethylene glycol that was kept at 264 K. This experiment did not have any complications, such as failed thermocouples, making the data from this pellet more reliable than the previous pellets discussed. This pellet was cut into two sections for imagining as shown in figure 49. In the center of this pellet one large crack occurred along with a smaller crack. These cracks are easily visible in the optical image.

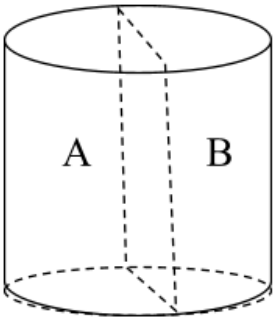

Figure 49. Imaging Diagram of U4-53C (Ortega, Yee, 2021)

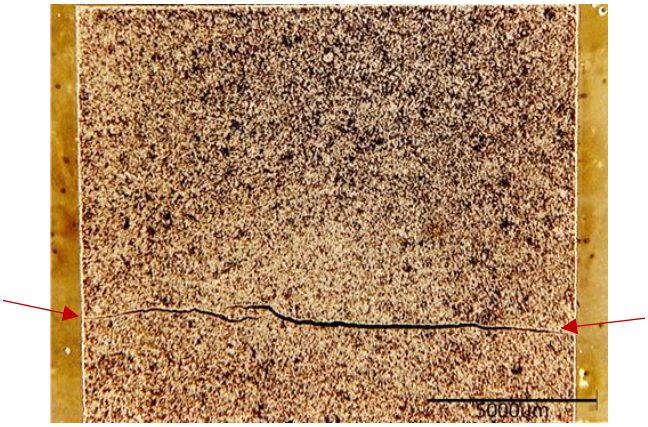

Figure 50. Optical Image of Section A of U4-53C (Ortega, Yee, 2021)

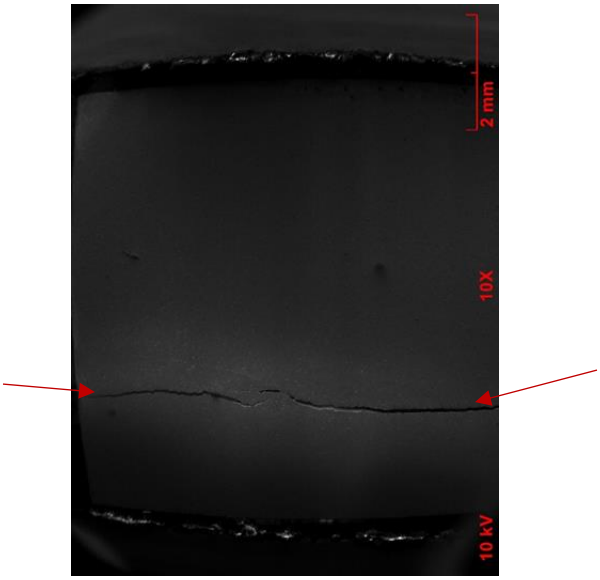

Figure 51. SEM Image of Section A of U4-53C (Ortega, Yee, 2021)

Some cracking also occurred on the bottom of the pellet. These cracks are very difficult to see on both the optical and SEM images.

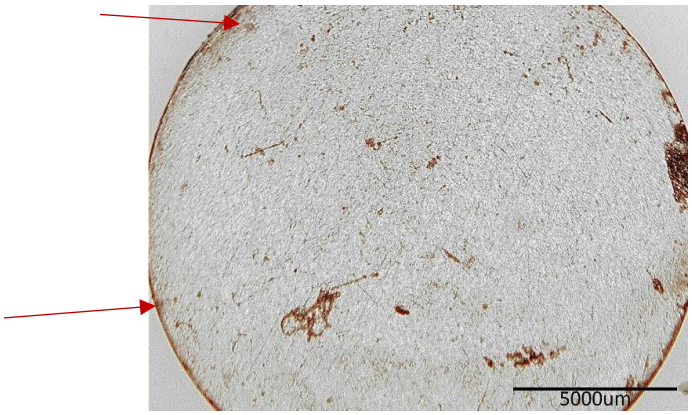

Figure 52. Optical Image of the Bottom of U4-53C (Ortega, Yee, 2021)

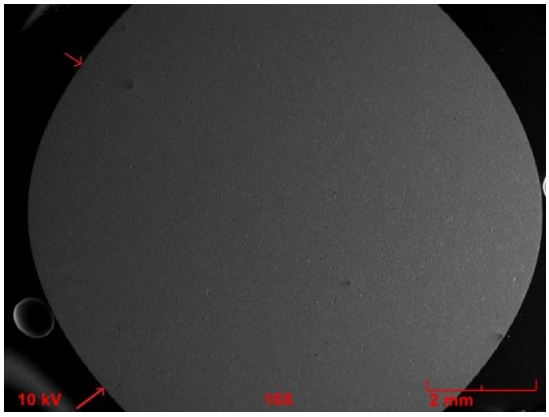

Figure 53. SEM Image of the Bottom of U4-53C (Ortega, Yee, 2021)

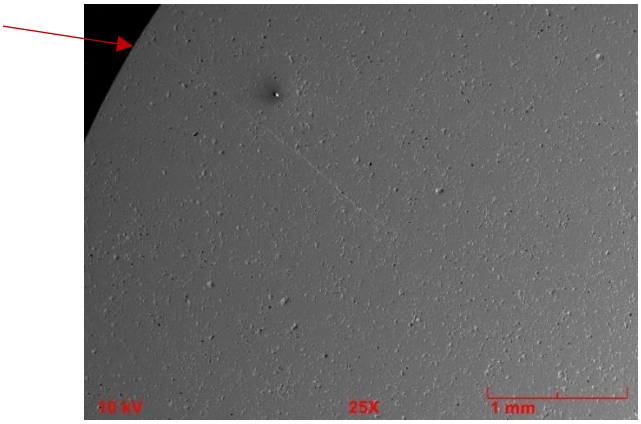

Figure 54. SEM Image of the Bottom of U4-53C Zoomed in on Crack 1 (Ortega, Yee, 2021)

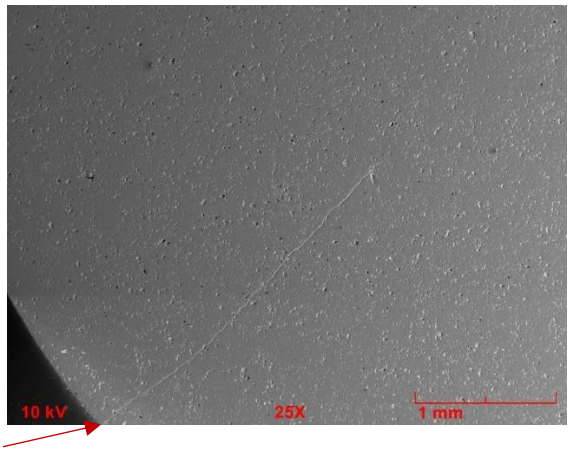

Figure 55. SEM Image of the Bottom of U4-53C Zoomed in on Crack 2 (Ortega, Yee, 2021)

The bottom of the pellet has only about one third of the cracking that occurred at the center. The center of the pellet had about 1.5 cm of cracking and the bottom of the pellet had about 0.5 cm of cracking for a total cracking length of 2.0 cm. This measured value is consistent with model predictions. The 2D models predicted 1.8 cm of cracking, about 90% of the experimental value. The 3D model predicted a total cracking length of just over 2.0 cm, or 100.6% of the actual cracking length.

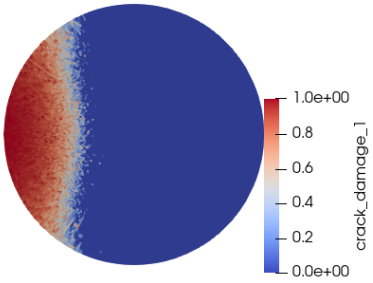

Figure 56.Predicted Axial Cracking of U4-53C

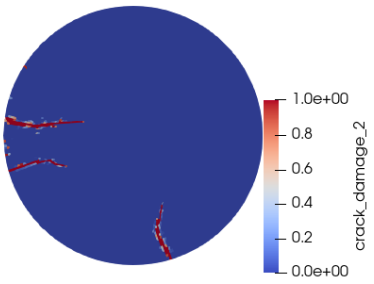

Figure 57.Predicted Radial Cracking U4-53C (Ortega, Yee, 2021)

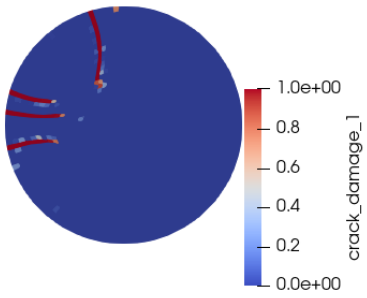

Figure 58.Predicted Cracking on Top of 3D Model of U4-53C

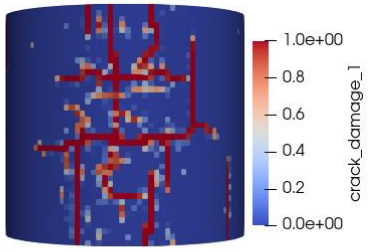

Figure 59. Predicted Cracking on Side of 3D model of U4-53C

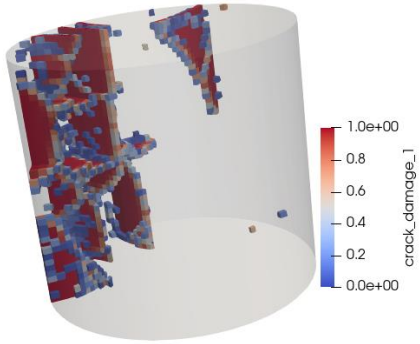

Figure 60. Filtered Predicted Cracking for U4-53C

5. U5-15A

Pellet U5-15A was 9.28 mm tall and had a diameter of 11 mm. The copper tube into which the pellet was placed was 180 mm tall, had an inner diameter of 14.5 mm and an outer diameter of 15.9 mm. Again, insulating material was used to push the pellet to one side of the copper tubing. The pellet-tube assembly was heated to 949 K, then quenched in an ice water bath kept at 277K. There were no known malfunctions during this experiment that would have compromised the results. This pellet was split into 3 sections for imaging as is shown in figure 61.

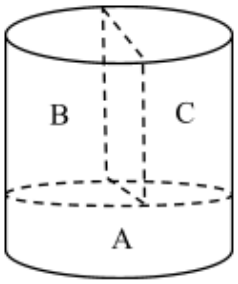

Figure 61. U5-15A Imaging Diagram (Ortega, Yee, 2021)

There was significant cracking in pellet section A, more than models predicted for the entire pellet. This amount of cracking is unusual in comparison to other experiments and raises questions about how representative the experimental results are.

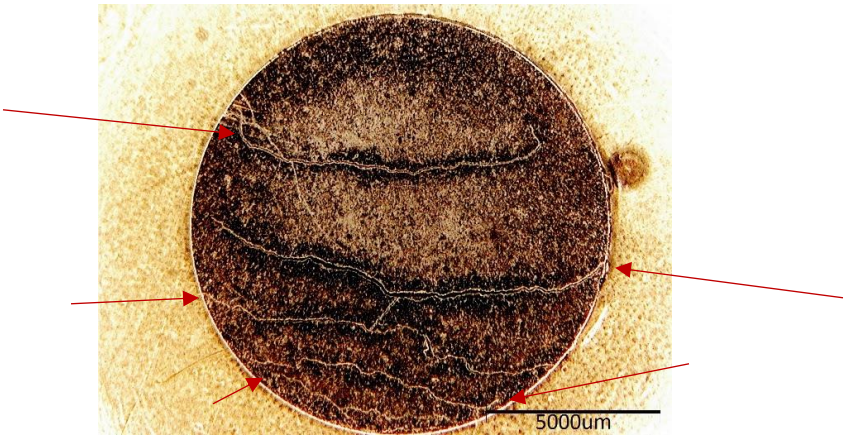

Figure 62. Optical image of U5-15A (Ortega, Yee, 2021)

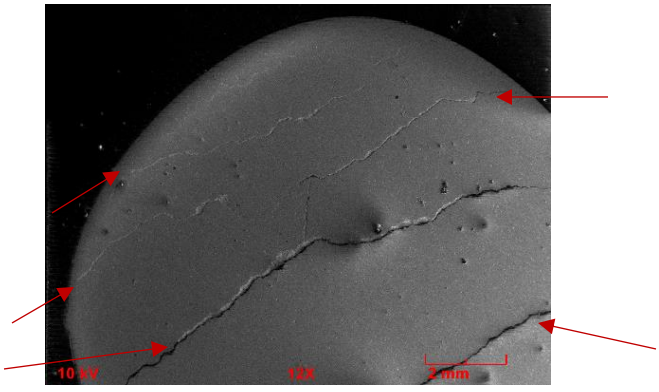

Figure 63. A SEM Image of U5-15A (Ortega, Yee, 2021)

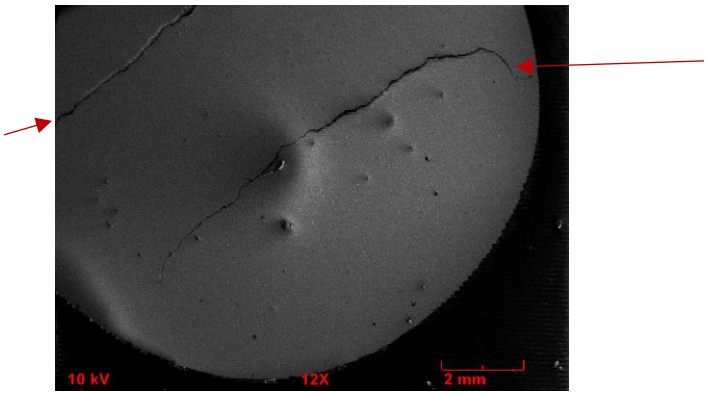

Figure 64. Another SEM Image of U5-15A (Ortega, Yee, 2021)

The cracking in section C is more in line with model predictions (Figures 65 and 66). The total crack length in this pellet experiment was 4.3 cm more than the models predicted.

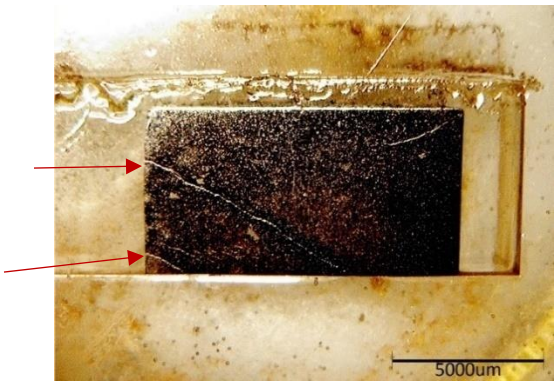

Figure 65. Optical Image of Section C of U5-15A (Ortega, Yee, 2021)

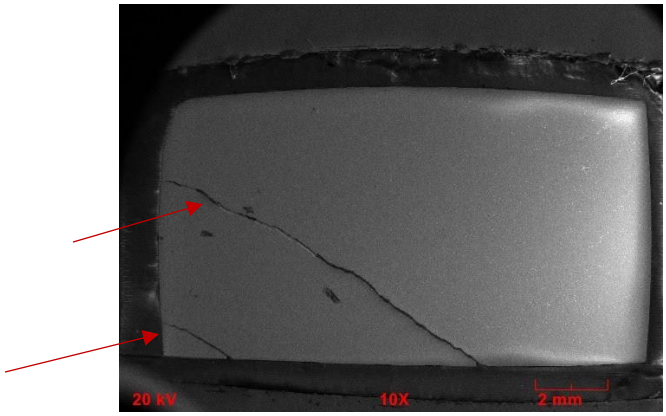

Figure 66. SEM Image of Section C of U5-15A (Ortega, Yee, 2021)

The model predicted about 1.8 cm of cracking, far less than actually occurred. That means the model is only accounting for 41.5%, far less than any of the experiments discussed to this point.

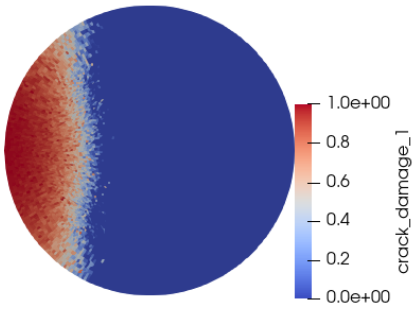

Figure 67 Predicted Axial Cracking of U5-15A

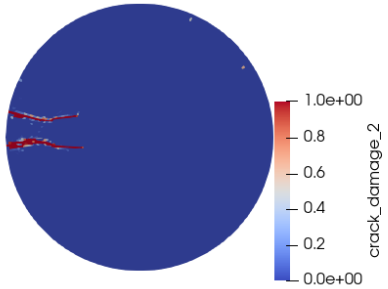

Figure 68. Predicted Radial Cracking of U5-15A

6. U2-49

Pellet U2-49 was 9.52 mm high and 11.02 mm in diameter. The copper tubing in which it was placed was 180 mm tall with an inner diameter of 14.5 mm and an outer diameter of 15.9 mm. Once again insulating material was used to push the pellet to one side of the tubing. The pellet-tube assembly was heated up to 942 K and quenched in an ice water bath that was kept at 277 K. There were no known malfunctions in this experiment that may compromise the results. This pellet was split into three sections for imaging as illustrated in figure 69.

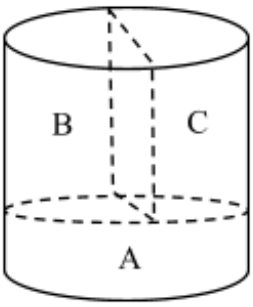

Figure 69. Imaging Diagram of U2-49 (Ortega, Yee, 2021)

While there were no known complications of this experiment, there was much less cracking than expected. As is shown in figure 70, little cracking is visible. The limited cracking may be explained a couple of ways. First, the results may simply represent the naturally random nature of cracking and of experimental results in a relatively small data. It's also possible the pellet was stronger than the others, which would be a result of variations from pellet to pellet. Another, more likely, explanation would be a flaw in the experiment. If the pellet was not making solid contact with the copper tubing, there would have been less heat transfer and less cracking than in other experiments. Figures 70 through 74 show little cracking. Section A has one crack that is fairly short, while sections B and C have a couple very short cracks. In total the total amount of cracking measured was 0.8 cm.

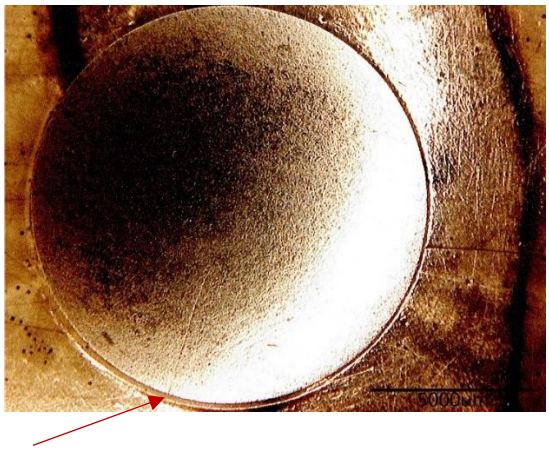

Figure 70. Optical Image of Section A of U2-49 (Ortega, Yee, 2021)

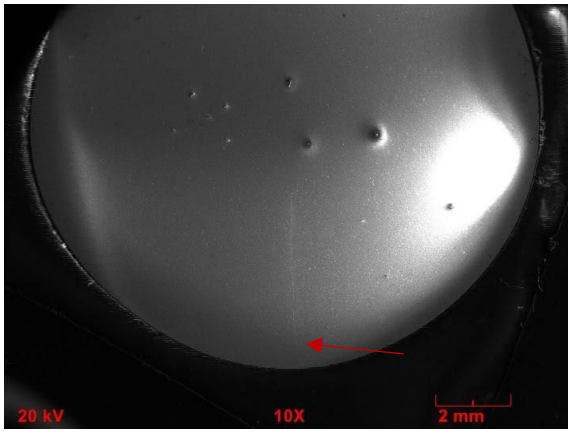

Figure 71. SEM Image of Section A of U2-49 (Ortega, Yee, 2021)

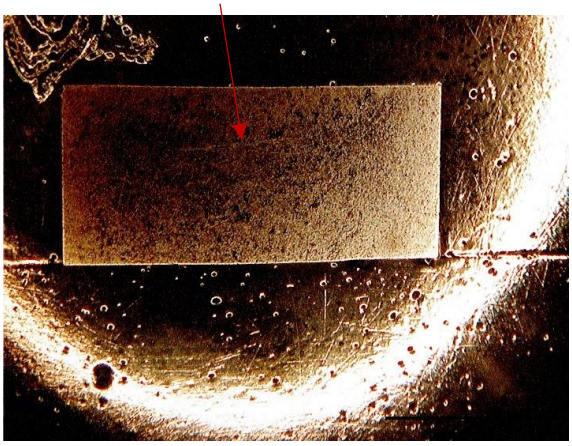

Figure 72. Optical Image of Section B of U2-49 (Ortega, Yee, 2021)

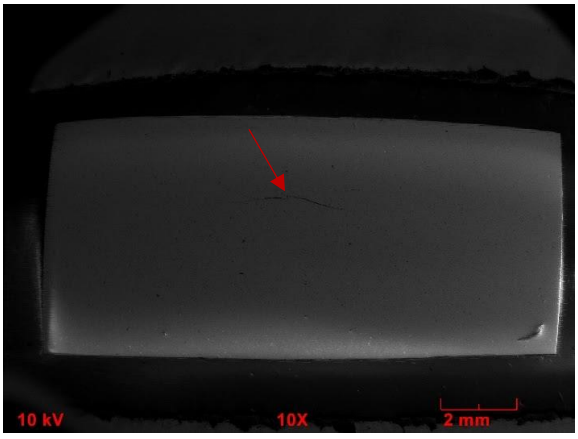

Figure 73. SEM Image of Section B of U2-49 (Ortega, Yee, 2021)

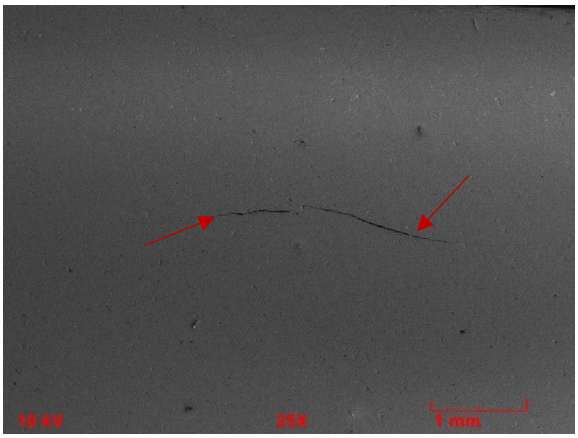

Figure 74. SEM Image of Section B of U2-49 Zoomed in on the Cracks (Ortega, Yee, 2021)

The 2D model of this experiment predicted more cracking than actually occurred. The predicted cracking is shown in figure 75 and 76. The model predicted 1.8 cm of cracking, 241% of the cracking that actually occurred in the experiment.

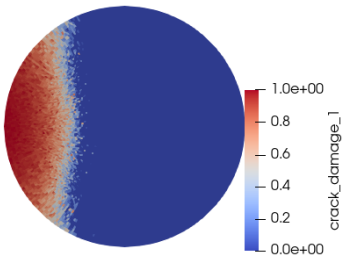

Figure 75. Predicted Axial Cracking of U2-49

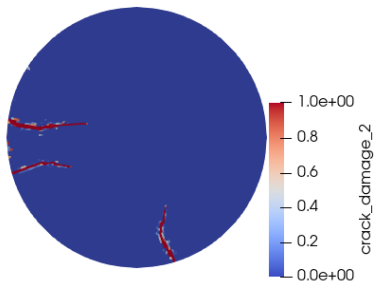

Figure 76. Predicted Radial Cracking of U2-49

7. Experiments That Did Not Crack

A few of the pellets did not crack during their experiments even though their models predicted cracking. As was discussed previously, there are a number of reasons that these pellets might not have cracked. The most likely cause is insufficient contact between the pellet and copper tubing, leading to insufficient heat transfer to produce the stresses needed to cause cracking.

a. U6-59

Pellet U6-59 was the first attempt at cracking a pellet via quenching. This pellet was 10.11 mm tall and 10.74 mm in diameter. The copper tube in which it was placed was 192.8 mm tall with a 11.3 mm inner diameter and a 12.7 mm outer diameter. This experiment was the only one to use $\frac{1}{2}$ inch copper tubing instead of $\frac{5}{8}$ inch copper tubing. The pellet had 135.65 mm of copper foil wrapped around the pellet to make contact with the copper tube. The pellet-tube assembly was heated to a relatively low temperature of 873 K, then quenched in a 50/50 mix of water and ethylene glycol kept at 264 K. The lack of cracking could have been for any number of reasons including the relatively low temperature, weak contact with the copper tubing, a combination or

something else. The 2D models predicted little axial cracking and one radial crack (Figures 77-79). The 3D model predicted slightly more cracking than the 2D model (Figures 80 and 81).

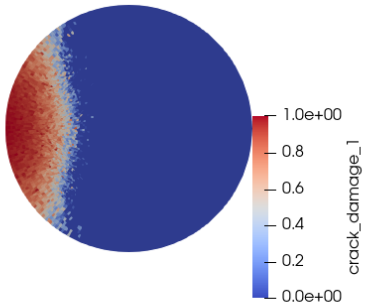

Figure 77. Predicted Axial Cracking of U6-59

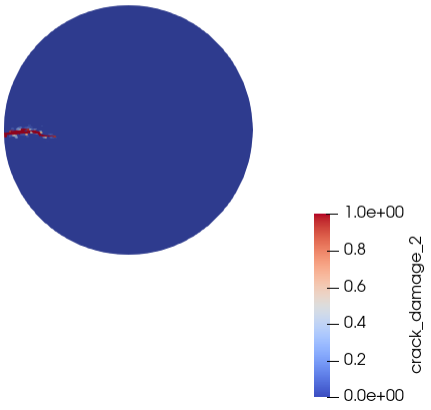

Figure 78. Predicted Radial Cracking of U6-59

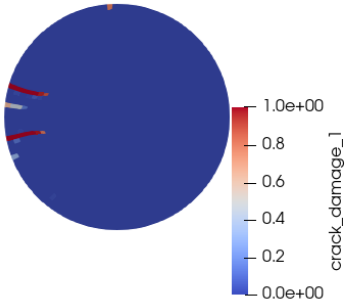

Figure 79. Predicted Cracking on Top of 3D Model of U6-59

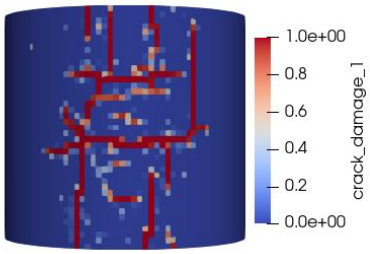

Figure 80. Predicted Cracking on the Side of the 3D Model of U6-59

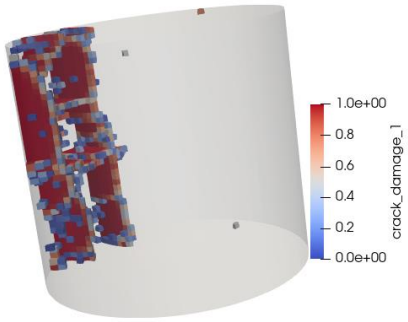

Figure 81. Filtered Predicted Cracking for U6-59

b. U2-25

Pellet U2-25 was 9.69 mm tall with a diameter of 11.24 mm. The copper tube in which it was placed measured 180 mm tall with a 14.5 mm inner diameter and 15.9 mm outer diameter. The pellet was pushed to one side of the tube with insulating material. Like U6-59, the high temperature of this pellet was low compared to the successfully cracked pellets. The pellet-tube assembly was heated to 873 K then quenched in a cold bath of 50/50 mixed water and ethylene glycol that was kept at 264 K. The thermocouples in this experiment failed. So, the data from this experiment is unreliable, because true temperatures are not known. Once again, the models predicted little cracking to occur (Figures 82-86).

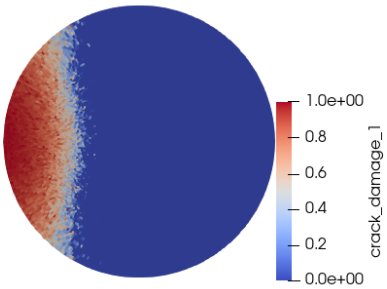

Figure 82. Predicted Axial Cracking of U2-25

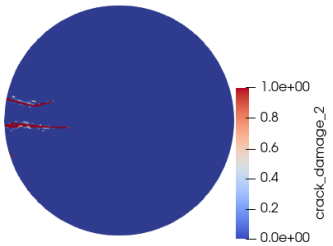

Figure 83. Predicted Radial Cracking of U2-25

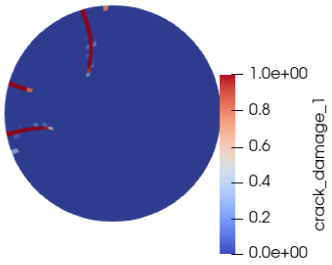

Figure 84. Predicted Cracking on the Top of the 3D Model for U2-25

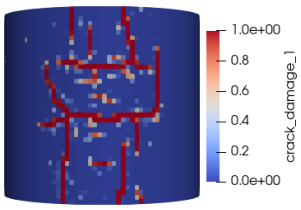

Figure 85. Predicted Cracking on the Side of the 3D Model for U2-25

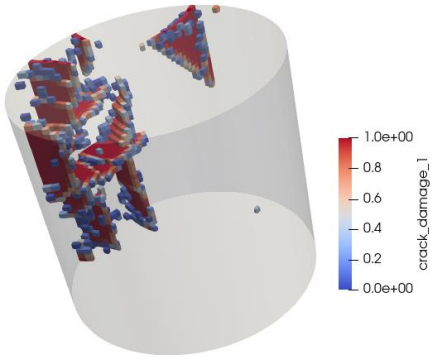

Figure 86. Filtered Predicted Cracking for U2-25

c. U4-42

Pellet U4-42 was 9.36 mm tall with a diameter of 11.04 mm. The copper tube in which it was placed measured 180 mm tall with an inner diameter of 14.5 mm and an outer diameter of 15.9 mm. The pellet was pushed against the side of the tube using insulating material. The pellet-tube assembly was heated to 859 K, which is lower than any of the pellets that cracked. Then it was quenched in an ice water bath that was kept at 277 K. The models of this experiment predicted a fair amount of cracking. There are several large radial cracks predicted in both 2D and 3D models (Figures 87-91). Given the accurate temperature data available for this experiment, the most likely explanation for the lack of cracking is that the amount of contact between pellet and copper pipe was less than needed.

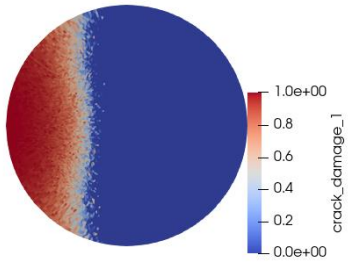

Figure 87. Predicted Axial Cracking of U4-42

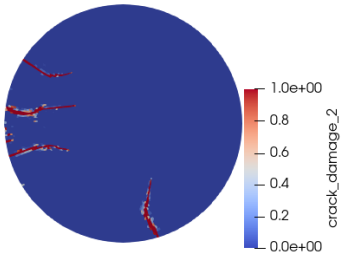

Figure 88. Predicted Radial Cracking of U4-42

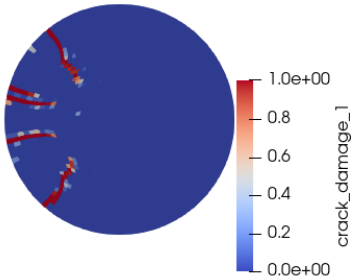

Figure 89. Predicted Cracking on Top of the 3D Model for U4-42

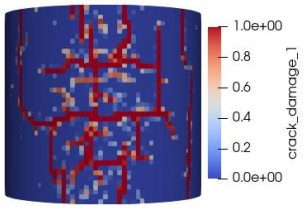

Figure 90. Predicted Cracking on Side of 3D Model of U4-42

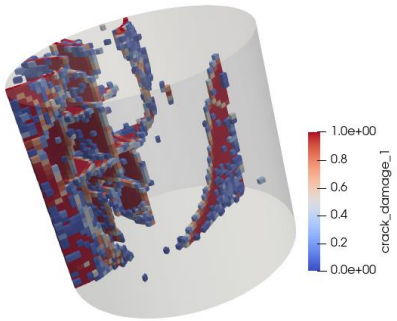

Figure 91. Filtered Predicted Cracking of U4-42

b. TREAT

i. 2D Smeared Cracking Model

A 2D model was developed to predict the fuel pellet cracking in the TREAT experiments. The schedule for conducting this experiment was pushed to later and later dates for a number of reasons beyond the control of this researcher. It was conducted shortly before this thesis was defended and no analysis of cracking was yet available. However, the models have been run and should still give an idea of what can be expected from the experiment. Five models were run at different power levels to match the experiment. The lowest power level for this experiment was 5 kW/m. At this power level, the models do not predict any cracking to occur but the amount of cracking rapidly increases with power as shown in figures 91 and 92. By 10 kW/m significant cracking is predicted. Figure 91 shows 4 substantial cracks in the pellet. The amount of cracking continues to grow with power level, until the highest power level in the experiment. As seen in figure 92, there is severe cracking at 25 kW/m.

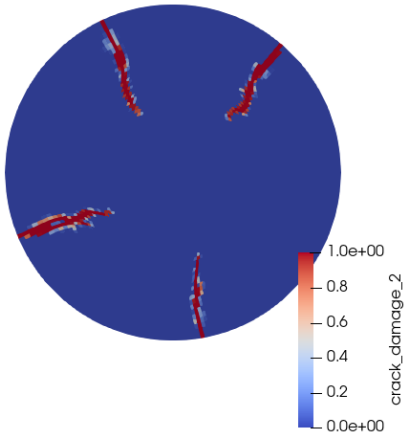

Figure 92. Predicted Cracking at 10 kW/m

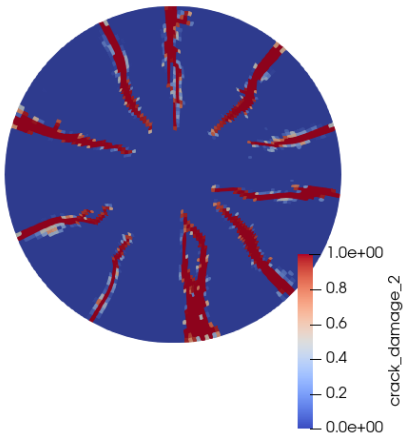

Figure 93. Predicted Cracking at 25 kW/m

Chapter 5. Summary

Work presented in this thesis was part of a multi-institutional project with objectives to perform experiments designed to produce data that can be used to validate the fuel cracking models in the Bison fuel performance code. Three types of experiments were performed at three different institutions, all with the objective of cracking UO_2 pellets: resistive heating experiments at University of South Carolina, quenching experiments at Texas A&M University, and fission heating in the TREAT facility at the Idaho National Laboratory (INL). These experiments were designed to produce the thermal gradient across that pellet that leads to cracking in new UO2 fuel pellets when first brough up to power in a Light Water Reactor (LWR). Modeling of these experiments, to inform experimental design and to compare to experimental results, was performed at Idaho State University and INL. Modeling performed for this thesis was largely in support of the temperature quenching experiments conducted at Texas A&M University, with a bit of modeling in support of the TREAT experiments.

In order to model the quenching experiments, it was necessary to determine the temperature dependent coefficient of heat transfer between the copper and the cold bath in which the heated pellet-copper assembly was quenched. A model was developed in MOOSE (the platform on which Bison is built) using a time dependent heat transfer coefficient function and was run allowing the heat transfer coefficient to be calculated. This was a slow tedious process. So, to speed up the run time for future model runs, a temperature dependent heat transfer coefficient function was developed. The model with the time dependent heat transfer coefficient was used to calculate the heat transfer coefficient between the copper and two cold bath options. Results of these runs indicated that an ice water bath had heat transfer properties similar to water-ethylene glycol, while

being less expensive. Therefore, all subsequent experiments conducted at Texas A&M use the water bath.

The next step in quench experiment modeling was to inform the experimenters of the minimum temperature required to create the stresses that would induce cracking. This modeling exercise consisted of adjusting the initial temperature on a Bison model, resulting in model output indicating a minimal cracking temperature of 450 K.

Smeared cracking models were run for every quenching experiment for which data was provided. A number of the experiments were compromised, resulting in unreliable data, but all were analyzed and presented in this thesis. The parameter chosen for comparison was total crack length. In general, the amount of pellet cracking predicted by the 3D models was more representative of actual cracking than that predicted by the 2D models. The 2D models predicted about 75% of the experimental cracking while 3D models predicted roughly 105% of the experimental cracking. Based on these results, it is expected that slight adjustment to the models, to better represent the physical experiments, will result in more accurate cracking predictions. In fact, the 2D model of the experiment with the most reliable results predicted 90% of the cracking and the 3D was almost perfect predicting 100.6% of the cracking.

At this point, the level of agreement between model predictions of cracking and experimentally measured cracking is not sufficient to justify Bison code validation. However, this work represents significant progress toward that goal and there is reason to believe that with some model adjustments, the code can be validated. Comparison of model predictions to the TREAT experiment results may represent another step toward the validation goal.

Chapter 6. Future Work

- Adjust quenching models to represent the experiments better.
- Compare the TREAT results with the models.
- Develop working models using XFEM approach, rather than smeared cracking, for both quenching and TREAT experiments.
- Compare XFEM predicts with experimental results.
- Run quenching models with pellet moving away from copper tube.

7. Bibliography

Burnett, D. J., & Schreyer, H. L. (2018). A mesh objective method for modeling crack propagation using the smeared crack approach. *International Journal for Numerical Methods in Engineering*, *117*(5), 574–603. https://doi.org/10.1002/nme.5968

Cervera, M., & Chiumenti, M. (2006). Smeared crack approach: back to the original track. *International Journal for Numerical and Analytical Methods in Geomechanics*, *30*(12), 1173–1199. https://doi.org/10.1002/nag.518

Chiang , S., & Faya, S. (1961). A SURVEY ON FUEL PELLET CRACKING AND HEALING PHENOMENA IN REACTOR OPERATION. Sao Paulo; CENTRO DE ENGENHARIA NUCLEAR.

Datta, D. (2013). Introduction to eXtended Finite Element (XFEM) Method. Nantes ; Ecole Centrale de Nantes

Hernandez-Morales B. (2013) "Characterization of Heat Transfer during Quenching." *Steel Heat Treating Fundamentals and Processes*.

Ortega, L., Yee, K. Personal Communications 2021

Olander, D. R. (2009). Nuclear Fuels: Present and Future. *Engineering Journal*, *13*(1), 1–28. https://doi.org/10.4186/ej.2009.13.1.1

Spencer, B. W., Woolstenhume, N. E., Emerson, L. A., Yeh, J.-Y., Imholte, D. D., Hill, C. M., Chapman, D. B., Jensen, C. B., Dunzik-Gougar, M. L., Knight, T. W., Besmann, T. M., Parnaik, S., McDeavitt, S. M., Ortega, L., Perez-Nunez, D., & Ban, H. (2019). EPARATE-EFFECTS VALIDATION EXPERIMENTS FOR MODELS OF FRACTURE IN CERAMIC NUCLEAR FUEL. *Top Fuel*, 516–525.

UCHIDA, T., SUNAOSHI, T., KATO, M., & KONASHI, K. (2011). Thermal Properties of UO2 by Molecular Dynamics Simulation. *Progress in Nuclear Science and Technology*, *2*, 598–602. https://doi.org/10.15669/pnst.2.598

U.S. Dept. of Energy. (1992). *Doe fundamentals handbook* (Vol. 2).

Van Brutzel, L., Dingreville, R., & Bartel, T.J. (2015). Nuclear fuel deformation phenomena. *State-of-the-Art Report on Multi-Scale Modelling of Nuclear Fuels*, 59–79.
Williamson, R. L., Hales, J. D., Novascone, S. R., Tonks, M. R., Gaston, D. R., Permann, C. J., Andrs, D., & Martineau, R. C. (2012). Multidimensional multiphysics simulation of nuclear fuel behavior. *Journal of Nuclear Materials*, *423*(1-3), 149–163. https://doi.org/10.1016/j.jnucmat.2012.01.012

Yeh, J. (2018) *Fuel Fracture Experimental Designs using Bison Fuel Performance Code for Out-of-Pile Separate-Effects Validation Experiments* [Master's thesis, Idaho State University]